

1
2
3
4 **Assessing origins of end-Triassic tholeiites from Eastern North America using hafnium**
5 **isotopes**
6
7

8 Lynne J. Elkins^{1, *}, Christine M. Meyzen², Sara Callegaro³, Andrea Marzoli², Michael Bizimis⁴
9

10
11
12 ¹ University of Nebraska-Lincoln, Lincoln, NE 68510; lelkins@unl.edu
13

14 ² Dipartimento di Geoscienze, Università degli Studi di Padova, Via G. Gradenigo, 6, 35131
15 Padova, Italy; andrea.marzoli@unipd.it, christine.meyzen@unipd.it
16

17 ³ Centre for Earth Evolution and Dynamics, University of Oslo, Oslo, Norway;
18 sara.callegaro@geo.uio.no
19

20 ⁴ University of South Carolina; mbizimis@geol.sc.edu
21

22 * Corresponding author: Lynne Elkins (lelkins@unl.edu)
23
24
25

26 **Key Points:**

- 27
- End-Triassic tholeiites from Eastern North America were likely products of melting
28 Paleozoic age, subduction-metasomatized mantle
 - Direct melting of recycled crustal rocks may also have occurred, but cannot fully explain
29 the tholeiite isotopic compositions observed
30
 - Southern Eastern North American tholeiites likely also experienced assimilation of lower
31 continental crust, possibly intermediate granulite
32

33 **Abstract**

34 The driving processes responsible for producing the Central Atlantic Magmatic Province, the
35 Large Igneous Province associated with end-Triassic rifting of Pangea, remain largely debated.
36 Because their compositions encompass most of the Central Atlantic basalt spectrum, tholeiites
37 from southern Eastern North America are considered pivotal for identifying magma origins. New
38 $^{176}\text{Hf}/^{177}\text{Hf}$ measurements for 201 Ma Eastern North American tholeiites dominantly record a
39 local petrogenetic history. Their ϵ_{Hf} ratios, corrected to an emplacement age of 201 Ma (-7.85 to
40 +5.86), form a positive but shallowly sloped array slightly deviating from the terrestrial array on
41 a ϵ_{Hf} vs. ϵ_{Nd} diagram. Comparison of $^{176}\text{Hf}/^{177}\text{Hf}$ to other isotope ratios and trace elements helps
42 to rule out several petrogenetic scenarios, particularly mixing of melts from global depleted or
43 enriched mantle components. In contrast, partial melting of subduction-metasomatized mantle
44 can explain the parental magma composition for southern Eastern North America. Such
45 metasomatism likely occurred during Paleozoic subduction around Pangea and may have been
46 dominated by sediment-derived fluid reactions. The observed $^{176}\text{Hf}/^{177}\text{Hf}$ vs. $^{143}\text{Nd}/^{144}\text{Nd}$ array
47 may reflect subsequent assimilation of lower continental crust, perhaps together with limited
48 direct melting of recycled continental crust in the asthenosphere. The proposed recycling
49 scenario does not specifically support or preclude a mantle plume origin for the Central Atlantic
50 Magmatic Province, but instead points toward the presence of a distinct local mantle source and
51 crustal assimilation processes during magma transport. Detailed understanding of these local
52 effects is needed in order to more accurately understand the origins of Large Igneous Provinces.

53

54 **Key words:** 8410 Geochemical modeling; 8137 Hotspots, large igneous provinces, and flood
55 basalt volcanism; 1040 Radiogenic isotope geochemistry; 1037 Magma genesis and partial

57 **1. INTRODUCTION**

58 The Triassic-Jurassic rifting of Pangea and subsequent opening of the central Atlantic Ocean
59 represent a major stage of a Wilson cycle, describing the formation and destruction of oceanic
60 basins and supercontinents (Wilson, 1966). Wilson's classic model drew directly on the central
61 Atlantic basin and its history of repeated closures and reopenings as a primary example of global
62 tectonic processes. End-Triassic rifting was associated with the emplacement of one of the most
63 voluminous continental flood basalt provinces in Earth history (Figure 1), the Central Atlantic
64 Magmatic Province (CAMP; Marzoli et al., 1999), an event significant enough to have likely
65 triggered the end-Triassic mass extinction (Capriolo et al., 2020; Cirilli et al., 2009; Davies et al.,
66 2017; Heimdal et al., 2018; Hesselbo et al., 2002; Marzoli et al., 2004). Major continental rifting
67 events in geologic history are commonly associated with the eruption of a large igneous province
68 (LIP), but the causal relationships linking rifts with LIPs remain unclear. The distinction and the
69 transition between passive and active rifting models has been the object of several studies (Burov
70 & Gerya, 2014; Courtillot et al., 1999; Koptev et al., 2015; Sengör & Burke, 1978), all seeking to
71 better understand what processes initiate rifting and what factors cause rifted margins to be
72 magma-rich or magma-poor (Gillard et al., 2017). Large igneous provinces may also record the
73 arrival of deep-seated mantle plumes at the base of the lithosphere, which could in turn act to
74 initiate rifting, but it has been difficult to fully reconcile plume head arrival with continental
75 rifting models in all settings (e.g., Carlson, 1991; Courtillot et al., 1999; Morgan, 1983; Saunders
76 et al., 2007).

77 One peculiarity of CAMP magmas is that they display an overall high degree of geochemical
78 heterogeneity, which has led researchers to propose diverse magma origins such as an upwelling
79 mantle plume (e.g., Cebriá et al., 2003; De Boer, 1992; Oyarzun et al., 1997; Wilson, 1997);

80 metasomatized subcontinental lithospheric mantle (SCLM) (e.g., Deckart et al., 2005; Merle et
81 al., 2011; Verati et al., 2005); and asthenosphere and/or SCLM modified by subduction-derived
82 materials (e.g., Alibert, 1985; Callegaro et al., 2013, 2017; Dorais et al., 2005; Dupuy et al.,
83 1988; Heatherington & Mueller, 1999; Marzoli et al., 2019; Merle et al., 2014; Pegram, 1990;
84 Whalen et al., 2015). These proposed origins have been likewise interpreted to indicate various
85 geodynamic scenarios (e.g., Marzoli et al., 2018, and references therein). As an additional source
86 of complexity, while some of the diverse magma types have been identified across the province,
87 other CAMP magma compositions vary from region to region (Marzoli et al., 2018). It remains
88 unclear whether these regional heterogeneities are derived from locally diverse asthenospheric or
89 continental lithospheric mantle sources, or inherited by assimilation of local continental
90 lithosphere by deeper, perhaps plume-derived primary magmas. Each scenario has distinct
91 implications for how end-Triassic rifting and associated LIP emplacement occurred. The
92 diversity of models further demonstrates the uncertainty about the origins of LIPs and their links
93 to continental rifts.

94 As an important component of this ongoing effort to understand the origins of CAMP, much
95 prior literature has been dedicated to the petrogenesis of CAMP basalts from Eastern North
96 America (ENA), but questions persist about the characteristics and origins of their primary melt
97 sources, and the role and importance of assimilation and crustal contamination in modifying
98 primitive melt compositions (e.g., Callegaro et al., 2013; Dorais & Tubrett, 2008; Dostal and
99 Dupuy, 1984; Dostal & Durning, 1998; Heatherington & Mueller, 1999; McHone, 2000; Merle
100 et al., 2014; Pegram, 1990; Puffer, 1992, 2001, 2003; Shellnutt et al., 2018; Tollo & Gottfried,
101 1992; Whalen et al., 2015). Because of the geochemical heterogeneity recorded by the tholeiites
102 from Georgia to Virginia in the southern part of ENA, which encompass most of the CAMP

103 geochemical spectrum, and taking advantage of the mineralogical sensitivity of the ^{176}Lu - ^{176}Hf
104 isotopic system with respect to clinopyroxene-garnet ratios, this study aims to place new
105 constraints on the formation of CAMP and of LIPs more generally.

106 **2. GEOLOGIC SETTING**

107 **2.1. Tectonic setting of CAMP**

108 The opening of the Central Atlantic oceanic basin started with end-Triassic rifting of the
109 supercontinent Pangea, an event associated with the regional emplacement of tholeiitic magmas
110 over an estimated total surface of 10^7 km² spanning present-day eastern North America, northern
111 South America, northwest Africa, and southwestern Europe (Figure 1) (Marzoli et al., 1999,
112 2018). Central Atlantic Magmatic Province emplacement occurred at ~201 Ma with a duration of
113 peak magmatic activity constrained to less than 0.6 Ma (e.g., Blackburn et al., 2013; Davies et
114 al., 2017; Deckart et al., 1997; Dunning & Hodych, 1990; Hames et al., 2000; Hodych &
115 Dunning, 1992; Jourdan et al., 2009; Knight et al., 2004; Marzoli et al., 2004, 2011, 2019;
116 Nomade et al., 2007; Sebai et al., 1991; Verati et al., 2005, 2007). At ca. 201.6 to 200.9 Ma,
117 several short-lived magmatic pulses occurred all over the CAMP and preceded continental break-
118 up by several million years (Blackburn et al., 2013; Davies et al., 2017; Knight et al., 2004).

119 **2.2. Models for CAMP formation**

120 The origins of LIPs and their relationship with continental rifting are subjects of long standing
121 debate (e.g., Bryan & Ernst, 2008; Carlson, 1991; Coffin & Eldholm, 1992; Kent, 1991; Morgan,
122 1983; Saunders et al., 2007). Many studies have invoked one or more mantle plumes as
123 triggering mechanisms for CAMP rifting and magmatism, invoking heat-driven lithospheric

124 erosion and thinning, wide-scale asthenospheric upwelling and melting in a plume head, broad
125 crustal magmatic emplacement, and possible localized focusing of regional extension in response
126 to plume impingement on the overlying plate (e.g., Cebriá et al., 2003; Hill, 1991; Lizarralde &
127 Holbrook, 1997; McHone, 1978; Morgan, 1983; Oyarzun et al., 1997; Ruiz-Martínez et al.,
128 2012; White & McKenzie, 1989; Wilson, 1997).

129 However, plume evidence related to the CAMP episode is ambiguous: the central Atlantic basin
130 does not include any hotspot tracks of early Jurassic age, and dike orientations and the near-
131 synchronous onset of magmatism from Bolivia to Spain are inconsistent with a centralized,
132 radiating plume impact (e.g., Davies et al., 2017; May, 1971; McHone, 2000; Verati et al., 2005).
133 Therefore, many studies have advocated for non-plume dynamical mechanisms for triggering
134 rifting and melting (e.g., Bédard, 1992; De Min et al., 2003; Holbrook & Kelemen, 1993;
135 Holbrook et al., 1994; Kontak, 2008; McHone, 2000). These alternative models for CAMP
136 invoke other melt generation mechanisms, such as subcontinental insulation heating and edge-
137 driven convection (e.g., Anderson, 1994; Coltice et al., 2007).

138 Geochemically, most CAMP magmas exhibit signatures enriched in incompatible trace elements,
139 with combined Pb-Sr-Nd-Os radiogenic isotopes indicating the involvement of one or more long-
140 lived source reservoirs with time-integrated incompatible trace element enrichment (e.g.,
141 Callegaro et al., 2013, 2014, 2017; Marzoli et al., 2019; Merle et al., 2011, 2014; Whalen et al.,
142 2015). While these geochemical patterns could indicate melt contributions from recycled
143 material entrained in a deep mantle plume, geochemical signatures such as LILE enrichments
144 and Nb depletions in CAMP are notably arc-like (e.g., De Min et al., 2003; Deckart et al., 2005;
145 Jourdan et al., 2003; Puffer, 2001).

146 The arc-like trace element signatures observed in CAMP magmas could indicate a unique local
147 mantle source composition, or may be derived from assimilation of continental lithosphere
148 during magma transport (Alibert, 1985; Bertrand, 1991; Bertrand et al., 1982; Cebriá et al., 2003;
149 Chabou et al., 2010; De Min et al., 2003; Deckart et al., 2005; Dupuy et al., 1988; Heatherington
150 & Mueller, 1999; Iacumin et al., 2003; Jourdan et al., 2003; Papezik et al., 1988; Pegram, 1990;
151 Puffer, 1992; Ragland et al., 1992; Tollo & Gottfried, 1992; Verati et al., 2005). A plume origin
152 for the Sr-Nd-Pb isotope systematics of CAMP is likewise problematic given the lack of Atlantic
153 OIBs with comparable signatures (e.g., Janney & Castillo, 2001; Pegram, 1990). A lack of
154 primitive (picritic) magmas in CAMP is a hindrance when defining the mantle source origins for
155 the LIP, but recent isotope analyses of ENA tholeiites suggest that for the least evolved magmas,
156 a SCLM or shallow asthenospheric mantle source modified by either subduction-derived fluids
157 or direct addition of subducted and/or delaminated continental crustal material is a viable
158 scenario (Callegaro et al., 2013, 2014; Merle et al., 2014; Shelnutt et al., 2018; Whalen et al.,
159 2015).

160 **2.3. The Eastern North America study area**

161 Eastern North American CAMP (Figure 1) hosts a particularly well-documented volcanic and
162 intrusive tholeiite series, including dike swarms, sills, and basaltic flows exposed from Georgia
163 (USA) to Newfoundland (Canada). The ENA series incorporate much of the observed
164 geochemical diversity of the overall province. The major CAMP lava piles are locally associated
165 with extensional grabens and half-grabens along what is now eastern North America. The
166 Hartford-Newark-Gettysburg-Culpeper basins of Massachusetts, Connecticut, New Jersey,
167 Pennsylvania, and Virginia host a series of three major volcanic episodes, including the oldest
168 Orange Mountain series, the intermediate-age Preakness series, and the youngest Hook Mountain

169 series (e.g., Puffer, 1992; Tollo & Gottfried, 1992). These units are matched by similarly dated
170 and geochemically identified basalts and feeder dikes in Canada (e.g., Kontak, 2008; Jourdan et
171 al., 2009; Pe-Piper & Piper, 1999) and Morocco (e.g., Bertrand et al., 1982; Marzoli et al., 2019).
172 Contrary to observations in Morocco and northern ENA, rift basins in southern Virginia, the
173 Carolinas, and Georgia do not preserve lava flows and are dominated instead by diabase dikes
174 and a few sills (e.g., Ragland et al., 1992; Weigand & Ragland, 1970).

175 Diabases and basalt flows from ENA are geochemically diverse, and detailed analysis has
176 indicated that multiple parental magmas with distinct differentiation, fractionation, and/or
177 assimilation paths are likely necessary to generate the geochemical variations observed (e.g.,
178 Tollo & Gottfried, 1992). Mantle potential temperatures extrapolated from high-Fo ($> Fo_{87}$)
179 olivine cores from these rocks have a maximum calculated value of 1480°C (Callegaro et al.,
180 2013; Herzberg & Gazel, 2009; Hole, 2015), well below anomalously high temperatures
181 calculated for the likely plume-related Deccan and Siberian LIPs, but at least 100 °C higher than
182 normal ambient upper mantle (Herzberg & Gazel, 2009; Sobolev et al., 2011). These moderately
183 high temperatures raise questions about the origins of that heat in the absence of a mantle plume;
184 one possibility is continental insulation beneath supercontinents (e.g., Coltice et al., 2007; Rey,
185 2015). Within this framework, the wide geochemical variability observed in ENA tholeiitic dikes
186 and sills makes it a particularly good focus region for placing new geochemical constraints on
187 the diversity of magma source origins and the process of continental flood basalt production
188 during rifting.

189 **2. METHODS**

190 **2.1. CAMP sample selection and preparation**

191 Tholeiitic basalt and diabase samples were selected to achieve a representative coverage across
192 the geochemical variability observed in trace elements and Sr-Nd-Pb isotopes for the southern
193 ENA region (12 samples), as well as targeted comparison to other regions within CAMP
194 including the northern ENA Newark basin (six samples), Sierra Leone (one sample), and
195 Morocco (one sample) (Table 1, Figure 1). The selected samples have relatively fresh, unaltered
196 appearances, with prior major and trace element results indicative of minimal crustal assimilation
197 or post-eruptive alteration (Callegaro et al., 2013, 2017; Marzoli et al., 2019; Merle et al., 2014).
198 Of these, two southern ENA samples (CS28 and CS57) were selected because they are
199 particularly Mg-rich (> 12 wt.% MgO) and are among the most primitive rocks ever recovered
200 from CAMP (Table 1; Callegaro et al., 2013). An exception to the above criteria is sample
201 NEW68 from the Preakness unit of the Newark Basin, which was selected because it is likely
202 crustally contaminated (Merle et al., 2014).

203 The samples analyzed for this study were all collected during prior research, and sampling
204 locations and previous geochemical measurements have been published elsewhere (Callegaro et
205 al., 2013, 2017; Marzoli et al., 2019; Merle et al., 2014) (Table 1). Prior to analysis for the
206 current study, any weathered rinds were removed by cutting with a trim saw. Fresh, visibly
207 unaltered material was then broken into finer pieces using a rock hammer, which was protected
208 with layers of clean plastic sheeting to prevent contamination. Sample material was then reduced
209 to small chips and powdered using an agate mortar and pestle. Larger samples with a sufficient
210 volume of material were further powdered using a Spex Shatterbox alumina grinding apparatus.
211 Samples were prepared in this manner either at the University of Padova or at the University of
212 Nebraska-Lincoln.

213 **2.2. Analytical methods**

214 Samples were analyzed for Hf isotopes in the Center for Elemental Mass Spectrometry, School
215 of Earth, Ocean, and Environment, University of South Carolina. An aliquot of 100 mg of rock
216 powder was weighed and digested in a Teflon-distilled HF:HNO₃ mixture in a 3:1 ratio. After
217 dissolution, the solution was dried repeatedly in 6N HCl, after which Hf was separated from
218 matrix elements using Eichrom LN-Spec Resin and methods after Munker et al. (2001). Hafnium
219 separates were analyzed by mass spectrometry methods using a Thermo Neptune multi-collector
220 inductively-coupled plasma mass spectrometer (MC-ICP-MS). Procedural blanks recorded Hf
221 concentrations under 50 pg, and analytical precision was within 0.0017% (2σ standard error) for
222 all measured samples (Table 2). Isotope compositions were corrected for mass fractionation
223 using $^{179}\text{Hf}/^{177}\text{Hf} = 0.7325$. The JMC-475 standard was determined to have $^{176}\text{Hf}/^{177}\text{Hf} =$
224 0.282152 ± 0.000004 (n = 10) for the first round of analyses and $^{176}\text{Hf}/^{177}\text{Hf} = 0.282142 \pm$
225 0.000007 (n = 10) for the second batch (Table 2). The data were corrected for instrumental bias
226 using a JMC-475 reference value of 0.282160. As an additional test of external reproducibility,
227 we analyzed a gabbroic sample from the Freetown Layered Complex (Sierra Leone) as a
228 replicate of an earlier measurement by Callegaro et al. (2017), using a separate dissolution. Our
229 newly measured $^{176}\text{Hf}/^{177}\text{Hf}$ ratio for this sample (0.282917 ± 0.000005 ; Table 2) is similar to the
230 prior published result (0.282937 ± 0.000012). The two results are slightly outside of 2σ
231 uncertainty with each other, however, which may be attributed to minor sample heterogeneity
232 and the measurement of separate sample dissolutions. Additional analytical details and standard
233 information can be found in Khanna et al. (2014), Mallick et al. (2015), and Frisby et al. (2016).

234 3. RESULTS

235 All data measured in this study have been age corrected to a crystallization age of 201 Ma using
236 Lu/Hf ratios previously published for these samples (Callegaro et al., 2013, 2017; Marzoli et al.,
237 2019; Merle et al., 2014) (Table 2); age-corrected isotopic ratios are hereafter indicated with
238 “201 Ma” notation. A conservative uncertainty of ~5% for the Lu/Hf ratio translates to less than
239 0.3 ϵ_{Hf} units of uncertainty in the initial isotopic composition for rocks of this age, and has no
240 effect on the conclusions of this study. Most samples from the southern ENA region form a
241 distinct array exhibiting a shallower slope (slope = 0.92 ± 0.12) than the terrestrial array
242 (Vervoort et al., 2011), being slightly shifted toward higher $\epsilon_{\text{Hf } 201\text{Ma}}$ ratios for a given $\epsilon_{\text{Nd } 201\text{Ma}}$
243 value (Table 2, Figure 2a). A notable exception is sample CS73 from Virginia, which plots along
244 the terrestrial array. The oblique trend relative to the terrestrial array defined by southern ENA
245 samples resembles trends previously observed for basalts from Hawaii (Blichert-Toft et al.,
246 1999; Salters et al., 2006) and the Karoo LIP (Jourdan et al., 2007) (Figure 2a). Southern ENA
247 $\epsilon_{\text{Hf } 201\text{Ma}}$ ratios also form a slightly positive correlation with $^{206}\text{Pb}/^{204}\text{Pb}_{201\text{Ma}}$ isotope ratios
248 (Callegaro et al., 2013) (Figure 2b). The latitudinal $\epsilon_{\text{Hf } 201\text{Ma}}$ profile between 34 and 37 °N shows
249 a decreasing southward gradient (Figure S1) toward more enriched (less radiogenic) isotope
250 ratios, with the exception of sample CS73.

251 In contrast with ENA samples, those from the Newark basin, Morocco, and Sierra Leone are
252 overall consistent with the global array (Vervoort et al., 2011) (Figure 2a). An exception is the
253 sample NEW68, a Preakness unit tholeiite selected for comparison due to its distinct
254 geochemical signature indicative of crustal assimilation (Merle et al., 2014); NEW68 has a
255 slightly higher $\epsilon_{\text{Hf } 201\text{Ma}}$ ratio for its $\epsilon_{\text{Nd } 201\text{Ma}}$ than other Newark basin basalts. Newark basin
256 samples exhibit a range of $\epsilon_{\text{Hf } 201\text{Ma}}$ values from ~0 to +5 (Figure S1).

257 4. DISCUSSION

258 The shallow slope of southern ENA tholeiites relative to the terrestrial array (Figure 2a, Table 2)
259 indicates a systematically increasing contribution from a low- ϵ_{Hf} source towards the south
260 (Figure S1). However, unlike previous data sets such as Hawaiian basalts (Blichert-Toft et al.,
261 1999; Salters et al., 2006) and the Karoo LIP (Jourdan et al., 2007), the southern ENA CAMP
262 array extends towards low $^{206}\text{Pb}/^{204}\text{Pb}_{201\text{Ma}}$ ratios at the low- $\epsilon_{\text{Nd } 201\text{Ma}}$ end of the array (Figure 2).
263 Below, we explore a series of melt mixing and assimilation scenarios and compare the outcomes
264 to the observed CAMP trace element and isotopic data, in an attempt to explain the origins of
265 these isotopic characteristics.

266 4.1. Crustal assimilation in Carolina tholeiites

267 As noted above, aside from a few samples, recent isotopic studies of ENA and other CAMP
268 rocks have indicated relatively minor crustal assimilation effects (up to 10% assimilation) in
269 ENA tholeiites (Callegaro et al., 2013; Merle et al., 2014; Whalen et al., 2015), which have
270 relatively low age-corrected $^{187}\text{Os}/^{188}\text{Os}_{201\text{Ma}}$ (0.128 – 0.187, mean 0.137) despite high
271 $^{87}\text{Sr}/^{86}\text{Sr}_{201\text{Ma}}$ (0.70438 - 0.71074, mean 0.70613), high $^{207}\text{Pb}/^{204}\text{Pb}_{201\text{Ma}}$ (15.54 - 15.67, mean
272 15.61), variable $^{206}\text{Pb}/^{204}\text{Pb}_{201\text{Ma}}$ (17.41 - 18.65, mean 18.23), and low $^{143}\text{Nd}/^{144}\text{Nd}_{201\text{Ma}}$ ratios
273 (0.51204 - 0.51251, mean 0.51230). However, due to a lack of Hf compositional and isotopic
274 data for the potential end-member continental assimilants in the ENA province, it is unclear what
275 effects up to 10% crustal assimilation may have had on the Hf isotope compositions of ENA
276 CAMP magmas. To evaluate the potential impacts of assimilation on the Hf data set, we
277 calculated the effects of assimilation-fractional crystallization on ENA basalts using energy-
278 constrained methods after Bohron and Spera (2001) and Spera and Bohron (2001) (Tables S1,

279 S2; Figure 3), and considered three potential assimilants: local upper continental crust, and both
280 mafic and intermediate-SiO₂, lower crustal granulite rocks. To simplify the scenarios tested, we
281 make several initial assumptions, including the temperatures, compositions, and energy
282 properties of the primary magma and three assimilants (see Tables S1, S2). Our calculations also
283 assume a primary magma composition resembling the most incompatible element-depleted,
284 southern ENA tholeiite measured in this study with respect to Hf (sample CS49, with low [Hf] =
285 1.3 ppm, high $\epsilon_{\text{Hf } 201\text{Ma}} = +5.86$) (Table 2).

286 To estimate the average composition of local upper continental crust, we used the mean
287 compositions of measured Carolina terrane crustal rocks from Pettingill et al. (1984) and Sinha et
288 al. (1996) and the data compilation of Whalen et al. (2015) (Table S1). The composition and age
289 of the lower basement of the Carolina terrane is less well-constrained. In general, while some
290 lower continental crust (LCC) may be Phanerozoic in age, many lower crustal rocks worldwide
291 are composed of Archean to Proterozoic Precambrian granulites with a range of mafic to felsic
292 compositions (e.g., Huang et al., 1995; Schmitz et al., 2004; Vervoort et al., 2000), and there is
293 isotopic evidence that local Carolina terrane LCC is dominantly Proterozoic in age (Ingle et al.,
294 2003). While a range of LCC ages is thus possible, here we focus on Proterozoic lower crustal
295 sources for the Carolina terrane. Most lower crustal granulites measured lie along the terrestrial
296 $\epsilon_{\text{Nd}}-\epsilon_{\text{Hf}}$ array (Vervoort et al., 2000), but some granulite xenoliths exhibit decoupling of ϵ_{Hf} from
297 ϵ_{Nd} , likely caused by the presence of cumulate or restite igneous minerals or by fractionation
298 during metamorphic mineral growth (Schmitz et al., 2004). The decoupling toward higher ϵ_{Hf}
299 relative to the terrestrial array is primarily observed in Proterozoic granulites (Huang et al., 1995;
300 Schmitz et al., 2004; Zartman et al., 2013), and so also may play a role in the Carolina terrane
301 (Ingle et al., 2003). As for major element compositions, while much of the LCC may be mafic,

302 Zhao and Guo (2019) and Guo et al. (2019) have observed that local Carolina LCC likely has an
303 overall intermediate SiO₂ content; we thus test both mafic and intermediate-SiO₂ LCC
304 compositions (Figure 3, Table S1). The mafic LCC composition used here resembles mafic
305 granulite xenoliths from Michigan (Zartman et al., 2013) with decoupled ϵ_{Hf} and ϵ_{Nd} ; alternative
306 assimilation trajectories for mafic granulites lying along the terrestrial array exhibited a poorer fit
307 and, for simplicity, are not shown. We assume that the intermediate granulite has comparatively
308 enriched (unradiogenic) Hf and Nd isotopes and resembles intermediate-SiO₂ granulite xenoliths
309 from South Africa and measured by Schmitz et al. (2004) (Table S1). Several Pb isotopic
310 compositions were tested for the LCC assimilation scenarios to determine the best fit to the
311 measured ENA CAMP data set (see Figure 3, Table S1, S2), considering the large span of Pb
312 isotopic ratios exhibited by the basement terranes previously accreted to ENA (Pettingill et al.,
313 1984; Sinha et al., 1996; Whalen et al., 2015). Because well-characterized intermediate-SiO₂
314 granulite xenoliths in the literature are largely peraluminous, a composition that may not be
315 representative of all lower crust, we further tested a more aluminum-poor composition based on
316 well-characterized, intermediate-SiO₂ granulites from Jonsa, Finland (Nehring et al., 2010);
317 however, the Finnish granulite composition likewise exhibited a poorer fit than the other results,
318 so for simplicity it is not shown.

319 We show our calculated crustal assimilation trajectories in Figure 3. Only the relatively enriched,
320 intermediate-SiO₂ granulite assimilant can account for most of the Hf-Nd isotopic variability
321 observed in our samples with 10% assimilation or less (Figure 3). Up to 10% assimilation of
322 Carolina terrane UCC rocks cannot explain most of the $\epsilon_{\text{Hf}}-\epsilon_{\text{Nd}}$ data array (Figure 3). Mafic LCC
323 assimilation trajectories deviate to much higher ϵ_{Hf} than our sample data (Figure 3) when using
324 the isotopically decoupled assimilant after Zartman et al. (2013), and none of the mafic granulite

325 Pb isotope compositions tested are able to explain our samples' Pb isotopes using only 10%
326 addition (see also Callegaro et al., 2013; Merle et al., 2014; Whalen et al., 2015). For
327 intermediate-SiO₂ LCC, the Pb isotope composition of an assimilant needs to be relatively
328 unradiogenic (e.g., ²⁰⁶Pb/²⁰⁴Pb ~17.0-17.3), but the assimilant must also have relatively
329 unradiogenic ¹⁷⁶Hf/¹⁷⁷Hf and ¹⁴³Nd/¹⁴⁴Nd compositions (Figure 3). Such a low ²⁰⁶Pb/²⁰⁴Pb
330 composition may be plausible when compared with the ranges measured in granulites from
331 Antarctica (Wysoczanski et al., 1995), Scotland (Halliday et al., 1993), and Michigan (Zartman
332 et al., 2013), which provide global examples of intermediate to felsic lower crustal granulites,
333 and also in light of the low ²⁰⁶Pb/²⁰⁴Pb signatures observed in some exposed Carolina terrane
334 rocks (granulites, charnockites, and anorthosites; Sinha et al., 1996).

335 All of our LCC assimilation calculations exhibit concave-down curvature in Figure 3, suggesting
336 that, e.g., Pb may generally be more significantly impacted than Hf by assimilation processes
337 because of its higher concentrations in granulitic basement relative to mantle-derived basalts
338 (e.g., Zartman et al., 2013). We further note that among our tested compositions, only a crustal
339 contaminant containing accessory zircon, like our intermediate-SiO₂ granulite composition, had
340 sufficiently high Hf partition coefficients to reproduce the isotope compositions observed in our
341 southern ENA data set with only 10% assimilation. In our calculations, the presence of minor
342 zircon in the assimilant rock also extends the compositions of magmas experiencing even minor
343 assimilation to more highly unradiogenic ε_{Hf} values (Figure 3). The role of accessory minerals in
344 magma assimilation processes is, however, presently unclear and likely to be more complex than
345 our models allow. For example, minerals like zircon may be effectively dissolved from country
346 rocks adjacent to mafic sills and dikes early in the melt-rock interaction process, depending on
347 local zircon abundance, grain size, and Zr saturation in the melt (e.g., Bindeman & Melnik,

348 2016). Melt-rock interaction between intruding magmas and granulitic country rocks is also
349 likely to be highly variable both spatially and over time, beyond the relatively simple calculated
350 scenarios shown in Figure 3. We thus only conclude that limited absorption of intermediate-
351 SiO₂, relatively isotopically enriched granulitic wallrock by primary CAMP tholeiitic magmas
352 may in part account for elevation of southern ENA samples above the terrestrial data array,
353 within the 10% assimilation constraint previously identified using Os isotopes (Callegaro et al.,
354 2013; Merle et al., 2014).

355 **4.2. Source origins of Eastern North American tholeiites**

356 While assimilation of crust may play a role in generating part of the isotopic variability observed,
357 some observations, such as the complex Pb isotope systematics, still favor additional mantle
358 source heterogeneity effects to fully explain the origins of ENA CAMP (Callegaro et al., 2013;
359 Merle et al., 2014; Whalen et al., 2015). Based on their distribution, much of the isotopic
360 variations observed in ENA CAMP tholeiite samples may require the involvement of multiple
361 distinct mantle sources (Figure 2). Below we explore current working hypotheses for
362 heterogeneous source origins of the southern ENA CAMP data set, including 1) global mantle
363 reservoirs, 2) SCLM, and 3) recently recycled crust in the local asthenosphere.

364 *4.2.1. Hypothesis 1: Global mantle reservoirs as a source for CAMP*

365 A technique for identifying possible plume-derived and/or long-lived mantle reservoirs for the
366 central Atlantic region is considering the end member basalt compositions observed in local
367 ocean island basalts, such as the Azores (Béguélin et al., 2017), Madeira (Geldmacher et al.,
368 2011), or Bermuda (Mazza et al., 2019), as well as Mesozoic MORB (Janney & Castillo, 2001)
369 and recently identified Eocene magmatism in the Appalachians (Mazza et al., 2017) (Figure 2).

370 However, prior research (e.g., Marzoli et al., 2019, and references therein) has consistently
371 shown that such end-members cannot explain all of the isotopic compositions observed in
372 CAMP, and indeed Atlantic intraplate basalts span a notably different compositional range than
373 that observed across the ENA CAMP data set.

374 Long-lived mantle components, such as depleted MORB mantle (DMM) and the most extreme
375 enriched mantle end-members (EM-1 and EM-2), define a broader range of isotopic
376 compositions, and their potential contribution in generating the observed trends in CAMP
377 compositions is examined here. This scenario resembles the proposed origin for many hotspot
378 volcanic centers and ocean islands, and would potentially suggest the presence in the melt zone
379 of materials transported from the deep mantle via a mantle plume. However, recent isotope
380 measurements of ENA CAMP have demonstrated that mixing of long-lived, global mantle
381 components in a heterogeneous mantle source is unable to fully explain the range of isotope
382 compositions observed, particularly for Pb isotope ratios (Callegaro et al., 2013, 2014, 2017;
383 Merle et al., 2011, 2014), and that outcome remains unchanged by our new Hf contributions as
384 demonstrated by our mixing calculations (Figures 4, 5). In those calculations, we test more
385 recent estimates for the isotopic compositions of EM-1 and EM-2 (e.g., Jackson and Dasgupta,
386 2008; Jackson et al., 2007; Table S1), which have less extreme Pb isotope compositions than,
387 e.g., earlier estimates that were used in prior CAMP studies (e.g., Whalen et al., 2015); our
388 results do not, however, achieve a better fit to ENA CAMP isotopic data than previous work. We
389 further note that while parts of our data set resemble partial melts of enriched mantle reservoirs
390 like EM-1 or EM-2, the trend of the southern ENA CAMP data array is inconsistent with the
391 sense of enrichment implied by mixing trajectories in Figures 4 and 5. In particular, the samples
392 with isotopic signatures towards the low- ϵ_{Hf} end of the data array (i.e., trending towards enriched

393 mantle) also exhibit relatively low Pb isotope ratios and thus appear to trend away from the same
394 end members in Pb-isotope space. This apparent mismatch indicates that additional partial melt
395 sources must be considered to fully explain the origins of southern ENA CAMP.

396 *4.2.2. Hypothesis 2: Melting of subcontinental lithospheric mantle*

397 It is possible that the lithospheric mantle beneath CAMP has experienced prior melting (e.g.,
398 during rifting of Laurussia) that may have left a depleted and refractory lithospheric mantle
399 residue. The moderately high temperatures calculated for CAMP (Herzberg & Gazel, 2009) may
400 have then been sufficient to cause melting of the refractory SCLM: at temperatures of 1480°C
401 and relatively low mantle pressures (1.5-2.0 GPa), Falloon and Danyushevsky (2000) predicted
402 6-12% melting of anhydrous harzburgite. This refractory mantle should be depleted in
403 incompatible trace elements and thus may resemble depleted asthenospheric mantle in trace
404 element and isotopic composition, making it difficult to uniquely identify. We note that in this
405 scenario, heating and melting of refractory lithosphere would need to be sufficiently widespread
406 to explain the large volume of magma likely deposited during CAMP. The total volume
407 emplaced remains unknown, but the province spans a total area of approximately 10^7 km², as
408 noted above. We further note that mantle temperatures sufficient to remelt refractory SCLM are
409 also sufficient to melt the more fertile underlying lherzolitic asthenosphere, and the geochemical
410 signatures of these two scenarios are expected to significantly overlap. Such asthenospheric
411 melting is likely to produce an additional volume of magma that would overwhelm the trace
412 element contribution from the less fertile, trace element depleted, harzburgitic lithospheric rocks.

413 On the other hand, supra-subduction zone SCLM, such as that produced during the assembly of
414 Pangea, is further expected to be variably infiltrated by metasomatic fluids that would impart a

415 more enriched trace element and isotopic composition. A metasomatized SCLM is thus an
416 alternative and more fertile melt source that has been suggested for CAMP tholeiites (e.g.,
417 Alibert, 1985; Bertrand, 1991; Bertrand et al., 1982; Cebriá et al., 2003; De Min et al., 2003;
418 Deckart et al., 2005; Dostal & Durning, 1998; Dupuy et al., 1988; Heatherington & Mueller,
419 1999; Jourdan et al., 2003; Marsh, 1987; Merle et al., 2011; Pegram, 1990; Puffer, 1992; Puffer,
420 2003), including high-TiO₂ CAMP magmas from Sierra Leone (Callegaro et al., 2017). In Sierra
421 Leone, high-TiO₂ gabbros of the Freetown Layered Complex exhibit an enriched isotopic
422 signature characterized by very high ²⁰⁷Pb/²⁰⁴Pb_{201Ma} ratios but low ²⁰⁶Pb/²⁰⁴Pb_{201Ma} (Figure 2). A
423 small amount of lamproite magma, inferred to derive from a local, subduction-metasomatized
424 SCLM source, was tested as a plausible contributor, mixed with a dominant asthenospheric melt
425 (Callegaro et al., 2017). A group of high-TiO₂ samples from South America (Merle et al., 2011)
426 with comparatively low ²⁰⁷Pb/²⁰⁶Pb (Figure 2) may also sample a distinct, localized mantle or
427 SCLM source (Merle et al., 2011). While a portion of the field for southern ENA CAMP Pb
428 isotope signatures overlaps with that of Sierra Leone gabbros (Figure 2), they are otherwise
429 distinct, having low TiO₂ contents, higher ⁸⁷Sr/⁸⁶Sr_{201Ma}, and lower ¹⁴³Nd/¹⁴⁴Nd_{201Ma} than the
430 Freetown gabbros.

431 Without local volcanic samples inferred to derive from SCLM melt sources, or SCLM-derived
432 local xenoliths for comparison, there are no regional Hf isotopic constraints for southern ENA
433 SCLM, making it difficult to directly test for SCLM melt contributions to southern ENA CAMP
434 basalts. Eastern North American CAMP was located farther from cratonic or peri-cratonic
435 settings than magmas from Brazil or Sierra Leone, though, suggesting SCLM is a less likely melt
436 source for ENA. We further note that although there are rare exceptions (e.g., Griffin et al.,
437 2000), global SCLM xenolith data largely have ε_{Hf} > +9 (Choi et al., 2008, 2010; Shaw et al.,

438 2007; Wittig et al., 2007, 2010) (Figure S2), making it difficult to explain the observed array
439 primarily by this mechanism. We cannot completely rule out an exotic, metasomatized
440 lithospheric mantle melt component influencing the composition of individual samples with
441 slightly elevated ϵ_{Hf} (Figure 2a), but based on prior work, we consider it an unlikely overall melt
442 source for low-TiO₂ LIP tholeiites.

443 *4.2.3. Hypothesis 3: Paleozoic crustal recycling in the asthenosphere beneath CAMP*

444 In a third scenario, we explore Paleozoic recycling of crustal material and production of a
445 modified mantle source beneath ENA, which is subsequently melted during the CAMP event.
446 Callegaro et al. (2013) suggested that ENA magmas may derive from direct melting of local
447 asthenosphere containing 1) depleted upper mantle, 2) recycled upper continental crustal rocks,
448 possibly as subducted Paleozoic terrigenous sediments associated with the assembly of Pangea,
449 and 3) lower continental crustal rocks, perhaps delaminated and locally reintroduced into the
450 convecting melt region (see e.g., Magni and Király, 2019). Whalen et al. (2015) suggested a
451 related scenario in which melts and/or aqueous fluids derived from subducted sediments
452 modified the local mantle melt source beneath ENA, with a stronger fluid-derived signature in
453 the south and more melt metasomatism recorded to the north. Below, we explore the constraints
454 that Hf isotopes would place on both models, and attempt to evaluate the possible role of
455 Paleozoic recycled crust in ENA CAMP magma generation.

456 *4.2.3.1. Paleozoic recycling of upper and lower continental crust.* Crustal recycling provides
457 possible explanations for an incompatible-element enriched source with notably high Lu/Hf
458 ratios, as implied by the radiogenic $\epsilon_{\text{Hf } 201\text{Ma}}$ relative to $\epsilon_{\text{Nd } 201\text{Ma}}$ observed in southern ENA
459 CAMP. As an initial test of melting a subduction-modified mantle source, we first consider

460 whether direct mixing of local depleted asthenospheric mantle melts with recycled upper and
461 local crust, i.e. the scenario suggested by Callegaro et al. (2013), can directly produce the
462 observed data array (Figure 6). As discussed above, most continental crustal rocks plot along the
463 terrestrial array, making it difficult to reproduce the southern ENA data trend. However, some
464 lower crustal mafic granulites may inherit a high, decoupled ϵ_{Hf} ratio due to the presence of
465 significantly old garnet with high Lu/Hf ratios (e.g., Blichert-Toft et al., 2005), similar to some
466 of the xenoliths measured by Zartman et al. (2013). If recycled, e.g., by delamination into the
467 asthenosphere, mafic LCC thus represents a plausible mantle source with elevated ϵ_{Hf} above the
468 mantle array in Figure 2a. However, an additional unradiogenic (enriched) Hf source lying closer
469 to the mantle array would then also be required to fully explain the observed ENA data. Upper
470 continental crust is typically more enriched in incompatible elements and should plot along the
471 mantle array (Table S1, Figures 2a, 4), making it a reasonable, additional recycled source and
472 possibly lending support to the suggested model of Callegaro et al. (2013). Upper crustal
473 material could have been introduced to the regional mantle by subduction of terrigenous marine
474 sediments; if local sediment deposition occurred near a subducting margin and was relatively
475 close to a weathering continental source, such sediments would closely resemble the average
476 composition of nearby continental terranes, as modeled by Callegaro et al. (2013).

477 However, we observe that direct mixing of melts from ambient asthenosphere with a typical DM
478 isotopic composition (Salters and Stracke, 2004; Workman and Hart, 2005) with recycled LCC
479 and UCC material is unable to explain the Hf and Pb isotopes measured for southern ENA
480 CAMP, at least within currently available constraints (e.g., Figure 2b). This is illustrated by the
481 isotopic compositions of the suggested end-members in Table S1 and Figure 2b, where we
482 identify a Proterozoic lower crustal end-member represented by mafic granulite Michigan

483 xenoliths (“Mafic LCC,” Zartman et al., 2013), an upper crust end-member represented by local
484 average Carolina terrane (“UCC”) ($^{206}\text{Pb}/^{204}\text{Pb}$ ranges between ca. 17.1 and 17.5 for Carolina
485 terrane rocks; Pettingill et al., 1984; Sinha et al., 1996), and ambient mantle modeled as a DM
486 component (“DMM”). In particular, crustal components with ϵ_{Hf} and ϵ_{Nd} values capable of
487 explaining the CAMP array do not span a sufficiently large range in Pb isotopic compositions to
488 explain the measured data (Figure 2).

489 *4.2.3.2. Paleozoic recycling and metasomatism of the asthenosphere.* Alternatively, Whalen et al.
490 (2015) suggested a scenario for the recycling of regional Paleozoic upper crustal sediments into
491 the subcontinental asthenosphere without invoking lower crustal delamination. By incorporating
492 subducted pelagic marine sediments, this scenario offers an alternative to recycled local UCC
493 from the Carolina terrane, one that notably plots above the mantle array; such a component may
494 thus alleviate the need for melting of exotic (i.e., with decoupled ϵ_{Hf} and ϵ_{Nd}) mafic Proterozoic
495 LCC rocks. Unlike our upper crust estimate for the Carolina terrane, weathered terrigenous
496 marine sediments have elevated Lu/Hf ratios due to the progressive removal of heavy detritus
497 minerals like zircon during continental weathering and differential river transport; the elevated
498 Lu/Hf ultimately produces high ϵ_{Hf} relative to ϵ_{Nd} in clay-rich marine pelagic sediments (Chauvel
499 et al., 2014; Garcon et al., 2013, 2014; Vervoort et al., 1999, 2011). Chauvel et al. (2008)
500 determined time-averaged ϵ_{Hf} and ϵ_{Nd} isotope compositions for typical subducted sediments,
501 which reside in the same part of the Hf-Nd isotope diagram as both marine Fe-Mn precipitates
502 and seawater (e.g., Albarede et al., 1998) (Figure 2a). As an alternative to the prior mixing
503 scenario with upper and lower continental crust, here we test mixing of partial melts of depleted
504 asthenosphere with a combination of 1) local Carolina terrane crust and 2) global average marine
505 sediments (GLOSS, after Plank and Langmuir (1998) and Chauvel et al. (2008); Table S1).

506 Specifically, we tested a Paleozoic marine sediment source subducted beneath the CAMP
507 province during the construction of Pangea at ~370 Ma, i.e., 170 Ma prior to the CAMP melting
508 event, after Merle et al. (2014), Callegaro et al. (2013), and Whalen et al. (2015).

509 In Figure 6a, where mixing results are reported along with our data, ternary mixing of depleted
510 mantle, Carolina UCC crust, and average global sediment cannot account for the Hf-Nd isotopic
511 variability observed in ENA samples. While trace element concentrations in recycled sources are
512 necessarily averages of heterogeneous materials, and a small change in the trace element budget
513 of upper crust, for example, may appear to resolve the observed discrepancy in mixing
514 trajectories, the end members are inconsistent between diagrams. That is, average global
515 subducted sediment has elevated ϵ_{Hf} relative to ϵ_{Nd} , similar to the southern ENA data array (e.g.,
516 Chauvel et al., 2008; Chen et al., 2013; Vervoort et al., 2011), but its highly radiogenic Pb
517 isotope ratios are inconsistent with our most extreme samples, which have the lowest $\epsilon_{\text{Nd } 201\text{Ma}}$
518 but also the least radiogenic $^{206}\text{Pb}/^{204}\text{Pb}_{201\text{Ma}}$ and $^{207}\text{Pb}/^{204}\text{Pb}_{201\text{Ma}}$. While contributions of melts
519 from recycled crustal rocks could thus explain some of the intermediate compositions observed
520 in the ENA CAMP data set, the scenario is a poor explanation for the most unradiogenic samples
521 with respect to $\epsilon_{\text{Hf } 201\text{Ma}}$.

522 A more plausible recycling hypothesis is the creation of a hybrid, metasomatised mantle source
523 by the addition of subduction-derived fluids to the peridotitic mantle wedge, which in turn
524 partially melts to produce local CAMP tholeiites. Whalen et al. (2015) suggested that the
525 subducted sediments in the subcontinental CAMP asthenosphere have dehydrated and/or melted,
526 producing fluids that metasomatically modified ambient peridotite. They further tied the nature

527 of the metasomatic fluid (aqueous fluid in the south vs. silicate melt in the north) to geographic
528 variations along the ENA subprovince as noted above.

529 Hafnium is primarily considered a tracer of melt and not aqueous fluid metasomatism in modern
530 arc environments (e.g., Kempton et al., 2018), because Hf is expected to have relatively low
531 aqueous solubility (e.g., Banks, 1950; Linnen, 1998). However, the relatively low fluid mobility
532 of Hf means dehydration of subducted sediments may produce a relatively high Lu/Hf
533 metasomatic fluid, such that a modified mantle may develop relatively high ϵ_{Hf} ratios over time
534 (e.g., Janney et al., 2005; Kempton et al., 2018). If northern ENA tholeiites record primarily melt
535 metasomatism while southern ENA tholeiites record ancient fluid metasomatism of the regional
536 mantle source, as posited by Whalen et al. (2015), southern ENA mantle could then have
537 developed variably high ϵ_{Hf} compared to ϵ_{Nd} , while northern ENA mantle did not, similar to our
538 observations; however, such a difference in fluid vs. melt metasomatic effects could be
539 confounded by other factors. For instance, subducted metasediments may include stable
540 metamorphic garnet, which could impact the Lu/Hf ratio of metasomatizing melts or fluids
541 derived from the subducted rocks (e.g., Kempton et al., 2018). Some lithospheric mantle
542 xenoliths that have experienced metasomatism also have extremely high ϵ_{Hf} ratios, unlike ENA
543 CAMP basalts (e.g., Armytage et al., 2015). The impact of metasomatic source effects on long-
544 term $^{176}\text{Hf}/^{177}\text{Hf}$ ratios is thus unclear and warrants more careful analysis.

545 Here we introduce a new model for calculating the trace element and isotope compositions of
546 both subduction-modified depleted mantle wedge and subsequent partial melts of that modified
547 mantle source (Table S4). In the model, three initial reservoirs are age-corrected to the time of
548 subduction recycling: 1) ambient peridotite asthenosphere after Salters and Stracke's (2004)

549 Depleted Mantle; 2) average global oceanic sediment similar to GLOSS (Chauvel et al., 2008;
550 Plank and Langmuir, 1998); and 3) altered oceanic crust (AOC) calculated from Atlantic drill
551 core compositions (Staudigel et al., 1996). The composition of a metasomatizing fluid is then
552 determined for a range of mixtures of 1) an AOC-derived aqueous fluid and 2) either a melt or an
553 aqueous fluid derived from subducted sediment. Trace element concentrations in all AOC and
554 sediment-derived fluids are calculated using mobility and partition coefficients after Kogiso et al.
555 (1997), Stracke et al. (2003), and Johnson and Plank (2000) (Table S3; see Supporting
556 Information). The composition of the modified wedge is then determined for 0-10% fluid
557 addition to the mantle, and across the full range of fluid mixtures. Next, the resulting modified
558 mantle composition is tracked for isotopic decay from the time of recycling and metasomatism
559 (370 Ma) until the time of melting (201 Ma) to determine the isotopic and trace element
560 compositions of the mantle during CAMP. Predicted trace element compositions in CAMP
561 basalts were determined using a simple modal batch melting model and melt fraction of 6%, with
562 garnet lherzolite mineral/melt partition coefficients and residual peridotite modes as in Table S3.

563 Results from the wedge metasomatism and melting model, shown in Figure 7, approach or
564 overlap with the most isotopically depleted southern ENA CAMP basalt composition (sample
565 CS49), as long as the subduction and recycling age is relatively young. The results shown in
566 Figure 7 assume a Paleozoic subduction age of 370 Ma, i.e. the recycling age previously
567 suggested by Merle et al. (2014), Callegaro et al. (2013), and Whalen et al. (2015). Recycling
568 ages older than Paleozoic subduction fail to reproduce the $\epsilon_{\text{Hf } 201\text{Ma}}$, $\epsilon_{\text{Nd } 201\text{Ma}}$, and Pb isotope
569 ratios observed in our basalts. Melting of a mantle source modified by a purely aqueous
570 metasomatic fluid and dominated by sediment-derived fluid (i.e., the AOC-derived fluid $\leq 25\%$
571 of the fluid mixture) can reasonably explain sample CS49 with less than 10% fluid addition,

572 although we note that the Pb isotope results shown in Figure 7c are close but not an exact fit to
573 the measured data at the lowest fluid addition values ($< 4\%$) that work best for ϵ_{Hf} and ϵ_{Nd}
574 isotopes.

575 We further note that for the most radiogenic Pb isotopes observed in ENA CAMP tholeiites,
576 mantle metasomatism dominated by aqueous fluid addition is a closer match than melt
577 metasomatism, even for some Newark basin samples (Figure 7c). This observation conflicts with
578 the suggestion of Whalen et al. (2015) that differences in Paleozoic subduction angles modified
579 the metasomatic regime from north to south beneath the North American margin, and that more
580 northerly ENA tholeiites were dominated by melt- and not aqueous fluid metasomatism of the
581 Paleozoic mantle. We would argue that while the exact proportions of fluid addition to the
582 mantle wedge may have been variable, a fluid-dominated metasomatic agent where most of the
583 fluid is derived from subducted sediments (i.e., only a limited proportion of the fluid is
584 contributed by AOC) provides a particularly good match to the radiogenic $^{206}\text{Pb}/^{204}\text{Pb}$ ENA end-
585 member (Figure 7).

586 *4.2.3.3. A hybrid recycling, metasomatism, and assimilation model for ENA CAMP.*

587 While the most primitive ENA CAMP magma analyzed here is in good agreement with
588 predictions for melting of metasomatized mantle, the remainder of our observed data array
589 cannot be explained purely by melting of such a source, even if the nature of that metasomatism
590 is itself regionally variable. Additional melting, mixing, and/or assimilation is thus required to
591 explain the full isotopic range exhibited by southern ENA CAMP. As explored above, the
592 compositions of southern ENA samples with low $\epsilon_{\text{Nd } 201\text{Ma}}$, comparatively radiogenic $\epsilon_{\text{Hf } 201\text{Ma}}$,
593 and relatively low $^{206}\text{Pb}/^{204}\text{Pb}_{201\text{Ma}}$ cannot be easily explained by melt mixing. Of the possible

594 sources considered here, only lower crustal granulites with decoupled Lu/Hf and Sm/Nd have the
595 necessary isotopic signatures to plausibly explain this composition, but the required proportional
596 contributions of melts from such a source are inconsistent in our calculations (Figure 8), and are
597 too large for some of the resulting mixtures to be basaltic in major element composition. Based
598 on the analysis above, we thus suggest that the ENA CAMP mantle melt source is dominated by
599 fluid-metasomatized asthenosphere, perhaps containing moderate quantities of recycled
600 continental crustal material, but not so much all of the observed data can be explained by direct
601 melting of those recycled rocks. Some minor (generally < 10%) assimilation of zircon-bearing,
602 intermediate-SiO₂, granulitic lower crust can then help to explain much of the southern ENA
603 data array (Figure 3). Our favored model thus includes a combination of factors, where some
604 direct melting of recycled crust is plausible, but minor crustal assimilation is also favored,
605 particularly to explain the southern ENA CAMP samples with the lowest $\epsilon_{\text{Hf } 201\text{Ma}}$ values. We
606 consider this a plausible model to explain the systematic trend towards low $\epsilon_{\text{Nd } 201\text{Ma}}$ and
607 $^{206}\text{Pb}/^{204}\text{Pb}_{201\text{Ma}}$ with comparatively high $\epsilon_{\text{Hf } 201\text{Ma}}$ and $^{207}\text{Pb}/^{204}\text{Pb}_{201\text{Ma}}$ in southern ENA basalts.

608 **4.3. Broader petrogenesis of Central Atlantic Magmatic Province tholeiites**

609 Figure 2a includes $^{176}\text{Hf}/^{177}\text{Hf}_{201\text{Ma}}$ results for magmas collected from other regions of CAMP,
610 including Sierra Leone and Morocco (Table 2). The range of isotopic compositions across
611 CAMP reflects localized processes, which for ENA include a local metasomatized mantle source
612 and minor assimilation of local crustal rocks. Such localized variations extend to other parts of
613 CAMP as well: samples from Sierra Leone, as noted above, exhibit notably high $\epsilon_{\text{Hf } 201\text{Ma}}$ values
614 for a given $^{206}\text{Pb}/^{204}\text{Pb}_{201\text{Ma}}$ ratio (Figure 2b) and have been suggested to incorporate melts from
615 local SCLM sources unique to that region, with an enriched composition comparable to

616 worldwide anorogenic lamproites, e.g. from Western Australia, Gausberg, or Leucite Hills
617 (Callegaro et al., 2017). Likewise, in Pb isotope space, most magmas from CAMP form an array
618 with high $^{207}\text{Pb}/^{204}\text{Pb}_{201\text{Ma}}$ for a given $^{206}\text{Pb}/^{204}\text{Pb}_{201\text{Ma}}$, while high-TiO₂ samples from South
619 America have comparatively lower $^{207}\text{Pb}/^{204}\text{Pb}_{201\text{Ma}}$ for a given $^{206}\text{Pb}/^{204}\text{Pb}_{201\text{Ma}}$ (Figure 2) (Merle
620 et al., 2011) and may instead sample a localized mantle or SCLM source, as noted above
621 (Deckart et al., 2005; Merle et al., 2011). Central Atlantic Magmatic Province rocks from
622 Guyana, Brazil, and Sierra Leone also include high-TiO₂ tholeiites (TiO₂ > 2 wt. %). The high-
623 TiO₂ CAMP magma type, which exhibits very distinct isotopic signatures and trace element
624 compositions (Marzoli et al., 2018), is volumetrically minor and confined to a narrow belt
625 bordering the Western African Craton and the Amazonia Craton/Guyana Shield (De Min et al.,
626 2003; Deckart et al., 2005; Dupuy et al., 1988; Mauche et al., 1989).

627 The above observations indicate that a number of isotopic patterns are unique to specific regions
628 within CAMP and sample localized sources in the underlying mantle. The more geographically
629 restricted patterns do not clearly indicate a radially distributed hotspot-like signature that might
630 directly support mantle plume influence. Even if the arrival of a plume head was associated with
631 more widespread geographic dispersal and magma emplacement across broader terranes (e.g.,
632 McHone, 1996), making geographic emplacement patterns far from radial, such episodes should
633 follow a sequence where first SCLM is melted due to thermal erosion, and then upwelling
634 asthenospheric mantle melts (e.g., Ernst & Buchan, 2003; Ernst et al., 2001; Morgan, 1983).
635 Based on isotope measurements and age information, neither scenario (geographically radial
636 distribution of isotopic enrichment, or timing sequences indicative of large-scale lithospheric
637 erosion and melting followed by asthenospheric melting) appears clear for CAMP.

638 Instead, the more localized geographic patterns appear to support regional upwelling and melting
639 of local mantle, including localized melting of SCLM for some areas. Our observations could
640 thus plausibly be explained either 1) by a regional passive upwelling response to lithospheric
641 thinning, i.e., localized mantle convection response to rift initiation, or 2) by the arrival of a deep
642 upwelling mantle plume and accompanying melting of entrained local asthenosphere and, in
643 some areas, overlying lithosphere. A province-wide geochemical plume signature for CAMP
644 thus remains ambiguous.

645 **5. CONCLUSIONS**

646 Eastern North American CAMP basalts were plausibly generated by melting of regionally
647 upwelling, depleted upper mantle asthenosphere, which was likely metasomatized by aqueous
648 fluids derived from subducted oceanic crust and marine sediments. That melting may have been
649 accompanied by direct melting of relatively minor quantities of previously recycled (e.g.,
650 subducted or delaminated) crustal rocks. Melting was likely then followed by assimilation of
651 lower continental crust, possibly intermediate-SiO₂ granulites containing minor accessory
652 minerals like zircon, which may influence the hafnium isotopic compositions of the basalts. The
653 isotopic compositions of CAMP basalts do not directly support dominantly OIB-like, long-lived,
654 enriched mantle source reservoir origins, but instead vary with local upper mantle and
655 lithospheric compositions across the province, recording broad, regional mantle upwelling. Our
656 findings thus suggest that continental rifting and the generation and emplacement of the CAMP
657 flood basalt province are best explained by regional asthenospheric decompression beneath the
658 Pangea supercontinent, neither requiring nor definitively precluding the influence of a deep-
659 seated mantle plume on continental rifting.

660 **Acknowledgments**

661 We thank Jörg Geldmacher, Pamela Kempton, and two anonymous reviewers for providing
662 thoughtful suggestions that helped improve a prior version of this manuscript. We also thank
663 John Lassiter and Steve Shirey for productive discussions about CAMP. Daren Blythe and
664 Nathan Sorsen assisted with sample preparation at UNL. L. Elkins acknowledges support from a
665 UNL College of Arts and Sciences International Collaboration Award that funded this research.
666 Field sampling was supported by the following grants: CARIPARO (Eccellenza 2008), PRIN
667 (PRIN 20158A9CBM), Padova University (CPDA132295/13) to A. M. N. Youbi (Caddi Ayyad
668 University, Marrakech, Morocco), H. Bertrand (ENS-Lyon, France), G. Bellieni (Padova
669 University, Italy), S. Howard (South Carolina Survey), and M. Higgins (North Carolina Survey)
670 are kindly thanked for help during fieldwork. Supporting data files are available at the IEDA data
671 repository (<https://doi.org/10.1594/IEDA/111347>).

672 **REFERENCES**

673 Albarede, F., A. Simonetti, J. D. Vervoort, J. Blichert-Toft, and W. Abouchami (1998), A Hf-Nd
674 isotopic correlation in ferromanganese nodules, *Geophysical Research Letters*, 25(20), 3895-
675 3898.

676 Alibert, C. (1985), A Sr-Nd isotope and REE study of late Triassic dolerites from the Pyrenees
677 (France) and the Messejana Dyke (Spain and Portugal), *Earth and Planetary Science Letters*,
678 73(1), 81-90.

679 Anderson, D. L. (1994), The sublithospheric mantle as the source of continental flood basalts:
680 The case against the continental lithosphere and plume head reservoirs, *Earth and Planetary*
681 *Science Letters*, 123, 269-280.

682 Armytage, R. M., A. D. Brandon, R. Andreasen, and T. J. Lapen (2015), Evolution of Mojavian
683 mantle lithosphere influenced by Farallon plate subduction: Evidence from Hf and Nd isotopes
684 in peridotite xenoliths from Dish Hill, CA, *Geochimica et Cosmochimica Acta*, 159, 264-284.

685 Baksi, A. K. (2003), Critical evaluation of $^{40}\text{Ar}/^{39}\text{Ar}$ ages for the Central Atlantic Magmatic
686 Province: timing, duration and possible migration of magmatic centers, *Geophysical Monograph*
687 *Series*, 136, 77-90.

688 Banks, H. O. (1950), The determination of the solubility of hafnium oxide in aqueous solution by
689 the radioactive tracer technique, 4822 pp, School of Mines and Metallurgy of the University of
690 Missouri, Rolla, Missouri.

691 Bédard, J. (1992), Jurassic quartz-normative tholeiite dikes from Anticosti Island, Quebec, In
692 *Eastern North American Mesozoic Magmatism*, Eds. Puffer, J.H. and P.C. Ragland, *Special*
693 *Papers-Geological Society of America*, v. 268, 161.

694 Begemann, F., K. Ludwig, G. Lugmair, K. Min, L. Nyquist, P. Patchett, P. Renne, C.-Y. Shih, I.
695 M. Villa, and R. Walker (2001), Call for an improved set of decay constants for
696 geochronological use, *Geochimica et Cosmochimica Acta*, 65(1), 111-121.

697 Béguelin, P., M. Bizimis, C. Beier, and S. Turner (2017), Rift–plume interaction reveals multiple
698 generations of recycled oceanic crust in Azores lavas, *Geochimica et Cosmochimica Acta*, 218,
699 132-152.

700 Bertrand, H. (1991), *The Mesozoic tholeiitic province of Northwest Africa; a volcanotectonic*
701 *record of the early opening of Central Atlantic*, In *Magmatism in extensional structural settings:*
702 *the Phanerozoic African Plate*, Eds. Kampunzu, A.B. and R.T. Lubala, Springer-Verlag, Berlin,
703 Germany.

704 Bertrand, H., J. Dostal, and C. Dupuy (1982), Geochemistry of early Mesozoic tholeiites from
705 Morocco, *Earth and Planetary Science Letters*, 58(2), 225-239.

706 Bindeman, I. N., and O. E. Melnik (2016), Zircon survival, rebirth and recycling during crustal
707 melting, magma crystallization, and mixing based on numerical modelling, *Journal of Petrology*,
708 57(3), 437-460.

709 Blackburn, T. J., P. E. Olsen, S. A. Bowring, N. M. McLean, D. V. Kent, J. Puffer, G. McHone,
710 E. T. Rasbury, and M. Et-Touhami (2013), Zircon U-Pb geochronology links the end-Triassic
711 extinction with the Central Atlantic Magmatic Province, *Science*, 340(6135), 941-945.

712 Blichert-Toft, J. (2001), On the Lu-Hf isotope geochemistry of silicate rocks, *Geostandards*
713 *Newsletter-the Journal of Geostandards and Geoanalysis*, 25(1), 41-56.

714 Blichert-Toft, J., F. A. Frey, and F. Albarede (1999), Hf isotope evidence for pelagic sediments
715 in the source of Hawaiian basalts, *Science*, 285(5429), 879-882.

716 Blichert-Toft, J., A. Agranier, M. Andres, R. Kingsley, J. G. Schilling, and F. Albarede (2005),
717 Geochemical segmentation of the Mid-Atlantic Ridge north of Iceland and ridge-hot spot
718 interaction in the North Atlantic, *Geochemistry Geophysics Geosystems*, 6,
719 10.1029/2004GC000788.

720 Bohron, W. A., and F. J. Spera (2001), Energy-constrained open-system magmatic processes II:
721 application of energy-constrained assimilation–fractional crystallization (EC-AFC) model to
722 magmatic systems, *Journal of Petrology*, 42(5), 1019-1041.

723 Bouvier, A., J. D. Vervoort, and P. J. Patchett (2008), The Lu–Hf and Sm–Nd isotopic
724 composition of CHUR: constraints from unequilibrated chondrites and implications for the bulk
725 composition of terrestrial planets, *Earth and Planetary Science Letters*, 273(1-2), 48-57.

726 Bryan, S. E., and R. E. Ernst (2008), Revised definition of large igneous provinces (LIPs), *Earth-*
727 *Science Reviews*, 86(1-4), 175-202.

728 Burov, E., and T. Gerya (2014), Asymmetric three-dimensional topography over mantle plumes,
729 *Nature*, 513(7516), 85.

730 Callegaro, S., A. Marzoli, H. Bertrand, M. Chiaradia, L. Reisberg, C. Meyzen, G. Bellieni, R. E.
731 Weems, and R. Merle (2013), Upper and lower crust recycling in the source of CAMP basaltic
732 dykes from southeastern North America, *Earth and Planetary Science Letters*, 376, 186-199.

733 Callegaro, S., D.R. Baker, A. De Min, A. Marzoli, K. Geraki, H. Bertrand, C. Viti, and F.
734 Nestola (2014), Enriched mantle source for the Central Atlantic magmatic province: New
735 supporting evidence from southwestern Europe, *Lithos*, 188, 15-32.

736 Callegaro, S., A. Marzoli, H. Bertrand, J. Blichert-Toft, L. Reisberg, G. Cavazzini, F. Jourdan,
737 J.H. Davies, L. Parisio, R. Bouchet, A. Paul, U. Schaltegger, M. Chiaradia (2017), Geochemical
738 Constraints Provided by the Freetown Layered Complex (Sierra Leone) on the Origin of High-Ti
739 Tholeiitic CAMP Magmas, *Journal of Petrology*, 58(9), 1811-1840.

740 Capriolo, M., A. Marzoli, L.E. Aradi, S. Callegaro, J. Dal Corso, R.J. Newton, B.J.W. Mills, P.B.
741 Wignall, O. Bartoli, D.R. Baker, N. Youbi, L. Remusat, R. Spiess, and C. Szabó, (2020), Deep
742 CO₂ in the end-Triassic Central Atlantic Magmatic Province, *Nature Communications* 11, 1670,
743 doi: 10.1038/s41467-020-15325-6.

744 Carlson, R. (1991), Physical and chemical evidence on the cause and source characteristics of
745 flood basalt volcanism, *Australian Journal of Earth Sciences*, 38(5), 525-544.

746 Cebriá, J. M., J. López-Ruiz, M. Doblas, L. T. Martins, and J. Munha (2003), Geochemistry of
747 the Early Jurassic Messejana-Plasencia dyke (Portugal-Spain); Implications on the Origin of the
748 Central Atlantic Magmatic Province, *Journal of Petrology*, 44, 547-568.

749 Chabou, M. C., H. Bertrand, and A. Sebaï (2010), Geochemistry of the Central Atlantic
750 Magmatic Province (CAMP) in south-western Algeria, *Journal of African Earth Sciences*, 58,
751 211-219.

752 Chauvel, C., E. Lewin, M. Carpentier, N. T. Arndt, and J. C. Marini (2008), Role of recycled
753 oceanic basalt and sediment in generating the Hf-Nd mantle array, *Nature Geoscience*, 1(1), 64-
754 67.

755 Chauvel, C., E. Lewin, M. Carpentier, N. T. Arndt, and J.-C. Marini (2008), Role of recycled
756 oceanic basalt and sediment in generating the Hf–Nd mantle array, *Nature geoscience*, 1(1), 64.

757 Chauvel, C., M. Garcon, S. Bureau, A. Besnault, B. M. Jahn, and Z. L. Ding (2014), Constraints
758 from loess on the Hf-Nd isotopic composition of the upper continental crust, *Earth and*
759 *Planetary Science Letters*, 388, 48-58.

760 Chen, T.-Y., G. Li, M. Frank, H.-F. Ling (2013), Hafnium isotope fractionation during
761 continental weathering: Implications for the generation of the seawater Nd-Hf isotope
762 relationships, *Geophysical Research Letters*, 40, 916-920.

763 Choi, S. H., S. B. Mukasa, X.-H. Zhou, X. H. Xian, and A. V. Andronikov (2008), Mantle
764 dynamics beneath East Asia constrained by Sr, Nd, Pb and Hf isotopic systematics of ultramafic
765 xenoliths and their host basalts from Hannuoba, North China, *Chemical Geology*, 248(1-2), 40-
766 61.

767 Choi, S. H., K. Suzuki, S. B. Mukasa, J. I. Lee, and H. Jung (2010), Lu-Hf and Re-Os
768 systematics of peridotite xenoliths from Spitsbergen, western Svalbard: Implications for mantle-
769 crust coupling, *Earth and Planetary Science Letters*, 297(1-2), 121-132.

770 Cirilli, S., A. Marzoli, L. Tanner, H. Bertrand, N. Buratti, F. Jourdan, G. Bellieni, D. Kontak, and
771 P. R. Renne (2009), Latest Triassic onset of the Central Atlantic Magmatic Province (CAMP)
772 volcanism in the Fundy Basin (Nova Scotia): New stratigraphic constraints, *Earth and Planetary
773 Science Letters*, 286, 514-525.

774 Coffin, M. F., and O. Eldholm (1992), Volcanism and continental break-up; a global compilation
775 of large igneous provinces, *Geological Society Special Publications*, 68, 17-30.

776 Coltice, N., B. Phillips, H. Bertrand, Y. Ricard, and P. Rey (2007), Global warming of the
777 mantle at the origin of flood basalts over supercontinents, *Geology*, 35(5), 391-394.

778 Courtillot, V., C. Jaupart, I. Manighetti, P. Tapponnier, and J. Besse (1999), On causal links
779 between flood basalts and continental breakup, *Earth and Planetary Science Letters*, 166, 177-
780 195.

781 Davies, J. H. F. L., A. Marzoli, H. Bertrand, N. Youbi, M. Ernesto, and U. Schaltegger (2017),
782 End-Triassic mass extinction started by intrusive CAMP activity, *Nature Communications*, 8,
783 15596.

784 De Boer, J. (1992), Stress configurations during and following emplacement of ENA basalts in
785 the northern Appalachians, In *Eastern North American Mesozoic Magmatism*, Eds. Puffer, J.H.
786 and P.C. Ragland, *Special Papers-Geological Society of America*, 268, 361.

787 De Min, A., E. M. Piccirillo, A. Marzoli, G. Bellieni, P. R. Renne, M. Ernesto, and L. S.
788 Marques (2003), The Central Atlantic Magmatic Province (CAMP) in Brazil: petrology,
789 geochemistry, $^{40}\text{Ar}/^{39}\text{Ar}$ ages, paleomagnetism and geodynamic implications, *Geophysical*
790 *Monograph Series*, 136, 91-128.

791 Deckart, K., G. Féraud, and H. Bertrand (1997), Age of Jurassic continental tholeiites of French
792 Guyana, Surinam and Guinea: Implications for the initial opening of the Central Atlantic Ocean,
793 *Earth and Planetary Science Letters*, 150, 205-220.

794 Deckart, K., H. Bertrand, and J.-P. Liégeois (2005), Geochemistry and Sr, Nd, Pb isotopic
795 composition of the Central Atlantic Magmatic Province (CAMP) in Guyana and Guinea, *Lithos*,
796 82, 289-314.

797 Dorais, M. J., and M. Tubrett (2008), Identification of a subduction zone component in the
798 Higganum dike, Central Atlantic Magmatic Province: A LA-ICPMS study of clinopyroxene with
799 implications for flood basalt petrogenesis, *Geochemistry, Geophysics, Geosystems*, 9(10).

800 Dorais, M. J., M. Harper, S. Larson, H. Nugroho, P. Richardson, and N. Roosmawati (2005), A
801 comparison of Eastern North America and Coastal New England magma suites: implications for
802 subcontinental mantle evolution and the broad-terrane hypothesis, *Canadian Journal Earth Sci*,
803 42(1571-1587).

804 Dostal, J., and C. Dupuy (1984), Geochemistry of the North Mountain Basalts (Nova Scotia,
805 Canada), *Chemical Geology*, 45(3), 245-261.

806 Dostal, J., and M. Durning (1998), Geochemical constraints on the origin and evolution of early
807 Mesozoic dikes in Atlantic Canada, *European Journal Mineralogy*, 10, 79-93.

808 Dunning, G. R., and J. P. Hodych (1990), U/Pb zircon and baddeleyite ages for the Palisades and
809 Gettysburg sills of the northeastern United States: Implications for the age of the
810 Triassic/Jurassic boundary, *Geology*, 18, 795-798.

811 Dupuy, C., J. Marsh, J. Dostal, A. Michard, and S. Testa (1988), Asthenospheric and lithospheric
812 sources for Mesozoic dolerites from Liberia (Africa): trace element and isotopic evidence, *Earth
813 and Planetary Science Letters*, 87(1), 100-110.

814 Eisele, J., M. Sharma, S. J. Galer, J. Blichert-Toft, C. W. Devey, and A. W. Hofmann (2002),
815 The role of sediment recycling in EM-1 inferred from Os, Pb, Hf, Nd, Sr isotope and trace
816 element systematics of the Pitcairn hotspot, *Earth and Planetary Science Letters*, 196(3), 197-
817 212.

818 Ernst, R. E., and K. L. Buchan (2003), Recognizing Mantle Plumes in the Geological Record,
819 *Annual Reviews Earth Planetary Science*, 31, 469-523.

820 Ernst, R. E., E. B. Grosfils, and D. Mège (2001), Giant Dike Swarms: Earth, Venus, and Mars,
821 *Annual Reviews Earth Planetary Science*, 29, 489-534.

822 Falloon, T.J. and L.V. Danyushevsky (2000), Melting of refractory mantle at 1.5, 2 and 2.5 GPa
823 under anhydrous and H₂O-undersaturated conditions: Implications for the petrogenesis of high-
824 Ca boninites and the influence of subduction components on mantle melting, *Journal of*
825 *Petrology*, 41(2), 257-283.

826 Frisby, C., M. Bizimis, and S. Mallick (2016), Hf-Nd isotope decoupling in bulk abyssal
827 peridotites due to serpentinization, *Chemical Geology*, 440, 60-72.

828 Garcon, M., C. Chauvel, C. France-Lanord, P. Huyghe, and J. Lave (2013), Continental
829 sedimentary processes decouple Nd and Hf isotopes, *Geochimica Et Cosmochimica Acta*, 121,
830 177-195.

831 Garcon, M., C. Chauvel, C. France-Lanord, M. Limonta, and E. Garzanti (2014), Which minerals
832 control the Nd-Hf-Sr-Pb isotopic compositions of river sediments?, *Chemical Geology*, 364, 42-
833 55.

834 Geldmacher, J., K. Hoernle, B. B. Hanan, J. Blichert-Toft, F. Hauff, J. B. Gill, and H.-U.
835 Schmincke (2011), Hafnium isotopic variations in East Atlantic intraplate volcanism,
836 *Contributions to Mineralogy and Petrology*, 162(1), 21-36.

837 Gillard, M., D. Sauter, J. Tugend, S. Tomasi, M.-E. Epin, and G. Manatschal (2017), Birth of an
838 oceanic spreading center at a magma-poor rift system, *Scientific reports*, 7(1), 15072.

839 Griffin, W., N. Pearson, E. Belousova, S. v. Jackson, E. Van Achterbergh, S. Y. O'Reilly, and S.
840 Shee (2000), The Hf isotope composition of cratonic mantle: LAM-MC-ICPMS analysis of
841 zircon megacrysts in kimberlites, *Geochimica et Cosmochimica Acta*, 64(1), 133-147.

842 Guo, W., S. Zhao, F. Wang, Z. Yang, S. Jia, and Z. Liu (2019), Crustal structure of the eastern
843 Piedmont and Atlantic coastal plain in North Carolina and Virginia, eastern North American
844 margin, *Earth, Planets and Space*, 71(1), 69.

845 Halliday, A. N., A. P. Dickin, R. N. Hunter, G. R. Davies, T. J. Dempster, P. J. Hamilton, and B.
846 G. Upton (1993), Formation and composition of the lower continental crust: evidence from
847 Scottish xenolith suites, *Journal of Geophysical Research: Solid Earth*, 98(B1), 581-607.

848 Hames, W. E., P. R. Renne, and C. Ruppel (2000), New evidence for geologically instantaneous
849 emplacement of earliest Jurassic Central Atlantic magmatic province basalts on the North
850 American margin, *Geology*, 28, 859-862.

851 Heatherington, A. L., and P. A. Mueller (1999), Lithospheric sources of North Florida, USA
852 tholeiites and implications for the origin of the Suwannee terrane, *Lithos*, 46, 215-233.

853 Heimdal, T. H., H. H. Svensen, J. Ramezani, K. Iyer, E. Pereira, R. Rodrigues, M. T. Jones, and
854 S. Callegaro (2018), Large-scale sill emplacement in Brazil as a trigger for the end-Triassic
855 crisis, *Scientific Reports*, 8, 141.

856 Heinonen, A., I. Mänttari, O.T. Rämö, T. Andersen, and K. Larjamo (2016), A prior evidence for
857 zircon antecryst entrainment in megacrystic Proterozoic granites, *Geology*, 44, 227-230.

858 Hermes, O. (1964), A quantitative petrographic study of dolerite in the Deep River Basin, North
859 Carolina, *Am. Mineral*, 49, 1718-1729.

860 Herzberg, C., and E. Gazel (2009), Petrological evidence for secular cooling in mantle plumes,
861 *Nature*, 458(7238), 619.

862 Hesselbo, S. P., S. A. Robinson, F. Surlyk, and S. Piasecki (2002), Terrestrial and marine
863 extinction at the Triassic-Jurassic boundary synchronized with major carbon-cycle perturbation:
864 A link to initiation of massive volcanism?, *Geology*, 30(3), 251-254.

865 Hill, R. I. (1991), Starting plumes and continental break-up, *Earth and Planetary Science*
866 *Letters*, 104(2), 398-416.

867 Hodych, J. P., and G. R. Dunning (1992), Did the Manicouagan impact trigger end-of-Triassic
868 mass extinction?, *Geology*, 20, 51-54.

869 Holbrook, W., and P. Kelemen (1993), Large igneous province on the US Atlantic margin and
870 implications for magmatism during continental breakup, *Nature*, 364(6436), 433-436.

871 Holbrook, W. S., E. Reiter, G. Purdy, D. Sawyer, P. Stoffa, J. Austin Jr, J. Oh, and J. Makris
872 (1994), Deep structure of the US Atlantic continental margin, offshore South Carolina, from
873 coincident ocean bottom and multichannel seismic data, *Journal of Geophysical Research*,
874 99(B5), 9155-9178.

875 Hole, M. J. (2015), The generation of continental flood basalts by decompression melting of
876 internally heated mantle, *Geology*, 43(4), 311-314.

877 Holm, P.M., J.R. Wilson, B.P. Christensen, L. Hansen, S.L. Hansen, K.M. Hein, A.K.
878 Mortensen, R. Pedersen, S. Plesner, and M.K. Runge (2006), Sampling the Cape Verde Mantle
879 Plume: Evolution of melt compositions on Santo Antão, Cape Verde Islands. *Journal of*
880 *Petrology*, 47, 145-189.

881 Huang, Y.-M., P. Van Calsteren, and C. I. Hawkesworth (1995), The evolution of the lithosphere
882 in southern Africa: a perspective on the basic granulite xenoliths from kimberlites in South
883 Africa, *Geochimica et Cosmochimica Acta*, 59(23), 4905-4920.

884 Iacumin, M., A. De Min, E. M. Piccirillo, and G. Bellieni (2003), Source mantle heterogeneity
885 and its role in the genesis of Late Archaean-Proterozoic (2.7-1.0 Ga) and Mesozoic (200 and 130
886 Ma) tholeiitic magmatism in the South American Platform, *Earth-Science Reviews*, 62, 365-397.

887 Ingle, S., P. A. Mueller, A. L. Heatherington, and M. Kozuch (2003), Isotopic evidence for the
888 magmatic and tectonic histories of the Carolina terrane: implications for stratigraphy and terrane
889 affiliation, *Tectonophysics*, 371(1-4), 187-211.

890 Jackson, M.G., S.R. Hart, A.P. Koppers, H. Staudigel, J. Konter, J. Blusztajn, M. Kurz, and J.A.
891 Russell (2007), The return of subducted continental crust in Samoan lavas, *Nature*, 448, 684-687.

892 Jackson, M. G., and R. Dasgupta (2008), Compositions of HIMU, EM1, and EM2 from global
893 trends between radiogenic isotopes and major elements in ocean island basalts, *Earth and*
894 *Planetary Science Letters*, 276(1-2), 175-186.

895 Jaffey, A. H., K. F. Flynn, Glendeni.Le, W. C. Bentley, and A. M. Essling (1971), Precision
896 Measurement of Half-Lives and Specific Activities of U-235 and U-238, *Physical Review C*,
897 4(5), 1889-1906.

898 Janney, P. E., and P. R. Castillo (2001), Geochemistry of the oldest Atlantic oceanic crust
899 suggests mantle plume involvement in the early history of the central Atlantic Ocean, *Earth and*
900 *Planetary Science Letters*, 192, 291-302.

901 Janney, P., A. Le Roex, and R. Carlson (2005), Hafnium isotope and trace element constraints on
902 the nature of mantle heterogeneity beneath the central Southwest Indian Ridge (13 E to 47 E),
903 *Journal of Petrology*, 46(12), 2427-2464.

904 Johnson, M. C., and T. Plank (2000), Dehydration and melting experiments constrain the fate of
905 subducted sediments, *Geochemistry, Geophysics, Geosystems*, 1(12), doi:
906 10.1029/1999GC000014.

907 Jourdan, F., A. Marzoli, H. Bertrand, M. Cosca, and D. Fontignie (2003), The northernmost
908 CAMP: $^{40}\text{Ar}/^{39}\text{Ar}$ age, petrology and Sr-Nd-Pb isotope geochemistry of the Kerforne dike,
909 Brittany, France, *Geophysical Monograph Series*, 136, 209-226.

910 Jourdan, F., H. Bertrand, U. Schärer, J. Blichert-Toft, G. Féraud, and A. B. Kampunzu (2007),
911 Major and trace element and Sr, Nd, Hf, and Pb isotope compositions of the Karoo Large
912 Igneous Province, Botswana-Zimbabwe: Lithosphere vs mantle plume contribution, *Journal of*
913 *Petrology*, 48(6), 1043-1077.

914 Jourdan, F., A. Marzoli, H. Bertrand, S. Cirilli, L. H. Tanner, D. J. Kontak, G. McHone, P. R.
915 Renne, and G. Bellieni (2009), $^{40}\text{Ar}/^{39}\text{Ar}$ ages of CAMP in North America: Implications for the
916 Triassic-Jurassic boundary and the ^{40}K decay constant bias, *Lithos*, 110, 167-180.

917 Kempton, P. D., H. Downes, and M. Lustrino (2018), Pb and Hf isotope evidence for mantle
918 enrichment processes and melt interactions in the lower crust and lithospheric mantle in Miocene
919 orogenic volcanic rocks from Monte Arcuentu (Sardinia, Italy), *Geosphere*, *14*(3), 926-950.

920 Kent, R. (1991), Lithospheric uplift in eastern Gondwana: Evidence for a long-lived mantle
921 plume system?, *Geology*, *19*(1), 19-23.

922 Khanna, T., M. Bizimis, G. Yogodzinski, and S. Mallick (2014), Hafnium-neodymium isotope
923 systematics of the 2.7 Ga Gadwal greenstone terrane, Eastern Dharwar craton, India:
924 Implications for the evolution of the Archean depleted mantle, *Geochimica Et Cosmochimica*
925 *Acta*, *127*, 10-24.

926 Klein, E. M. (2004), Geochemistry of the Igneous Ocean Crust, in *Treatise on Geochemistry*,
927 edited by H. D. Holland and K. K. Turekian, pp. 433-463, Elsevier, Amsterdam.

928 Klügel, A., K. Galipp, K. Hoernle, F. Hauff, and S. Groom (2017), Geochemical and
929 volcanological evolution of La Palma, Canary Islands. *Journal of Petrology*, *58*, 1227-1248.

930 Knight, K. B., S. Nomade, P. R. Renne, A. Marzoli, H. Bertrand, and N. Youbi (2004), The
931 Central Atlantic Magmatic Province at the Triassic-Jurassic boundary: paleomagnetic and
932 $^{40}\text{Ar}/^{39}\text{Ar}$ evidence from Morocco for brief, episodic volcanism, *Earth and Planetary Science*
933 *Letters*, *228*, 143-160.

934 Kogiso, T., Y. Tatsumi, and S. Nakano (1997), Trace element transport during dehydration
935 processes in the subducted oceanic crust: 1. Experiments and implications for the origin of ocean
936 island basalts, *Earth and Planetary Science Letters*, *148*(1-2), 193-205.

937 Kontak, D. J. (2008), On the edge of CAMP: Geology and volcanology of the Jurassic North
938 Mountain Basalt, Nova Scotia, *Lithos*, 101, 74-101.

939 Koptev, A., E. Calais, E. Burov, S. Leroy, and T. Gerya (2015), Dual continental rift systems
940 generated by plume–lithosphere interaction, *Nature Geoscience*, 8(5), 388.

941 Linnen, R. L. (1998), The solubility of Nb-Ta-Zr-Hf-W in granitic melts with Li and Li + F;
942 constraints for mineralization in rare metal granites and pegmatites, *Economic Geology*, 93,
943 1013-1025.

944 Lizarralde, D., and W. S. Holbrook (1997), US mid-Atlantic margin structure and early thermal
945 evolution, *Journal of Geophysical Research*, 102, 22.

946 Magni, V. and A. Király (2019), Delamination, Reference Module in Earth Systems and
947 Environmental Sciences, Elsevier.

948 Mallick, S., J. J. Standish, and M. Bizimis (2015), Constraints on the mantle mineralogy of an
949 ultra-slow ridge: Hafnium isotopes in abyssal peridotites and basalts from the 9-25°E Southwest
950 Indian Ridge, *Earth and Planetary Science Letters*, 410, 42-53.

951 Marsh, J. S. (1987), Basalt geochemistry and tectonic discrimination within continental flood
952 basalt provinces, *Journal of Volcanology and Geothermal Research*, 32(1-3), 35-49.

953 Marzoli, A., P. R. Renne, E. M. Piccirillo, M. Ernesto, G. Bellieni, and A. De Min (1999),
954 Extensive 200-Million-Year-Old Continental Flood Basalts of the Central Atlantic Magmatic
955 Province, *Science*, 284, 616-618.

956 Marzoli, A., H. Bertrand, K.B. Knight, S. Cirilli, C. Verati, S. Nomade, P.R. Renne, N. Youbi, R.
957 Martini, K. Allenbach, R. Neuwerth, C. Rapaille, L. Zaninetti, and G. Bellieni (2004), Synchrony
958 of the Central Atlantic magmatic province and the Triassis-Jurassic boundary climatic and biotic
959 crisis, *Geology*, 32, 973-976.

960 Marzoli, A., F. Jourdan, J. H. Puffer, T. Cuppone, L. H. Tanner, R. E. Weems, H. Bertrand, S.
961 Cirilli, G. Bellieni, and A. De Min (2011), Timing and duration of the Central Atlantic magmatic
962 province in the Newark and Culpeper basins, eastern U.S.A., *Lithos*, 122, 175-188.

963 Marzoli, A., F. Jourdan, F. Bussy, M. Chiaradia, and F. Costa (2014), Petrogenesis of tholeiitic
964 basalts from the Central Atlantic magmatic province as revealed by mineral major and trace
965 elements and Sr isotopes, *Lithos*, 188, 44-59.

966 Marzoli, A., S. Callegaro, J. Dal Corso, J. H. F. L. Davies, M. Chiaradia, N. Youbi, H. Bertrand,
967 L. Reisberg, R. Merle, and F. Jourdan (2018), The Central Atlantic Magmatic Province (CAMP):
968 A Review, in *The Late Triassic World: Earth in a Time of Transition*, edited by L. H. Tanner, pp.
969 91-125, Springer International Publishing, Cham.

970 Marzoli, A., H. Bertrand, N. Youbi, S. Callegaro, R. Merle, L. Reisberg, M. Chiaradia, S.
971 Brownlee, F. Jourdan, and A. Zanetti (2019), The Central Atlantic magmatic province (CAMP)
972 in Morocco, *Journal of Petrology*, 60, 945-996.

973 Mauche, R., G. Faure, L. M. Jones, and J. Hoefs (1989), Anomalous isotopic compositions of Sr,
974 Ar and O in the Mesozoic diabase dikes of Liberia, West Africa, *Contributions to Mineralogy
975 and Petrology*, 101(1), 12-18.

976 May, P. R. (1971), Pattern of Triassic-Jurassic Diabase Dikes around the North Atlantic in the
977 Context of Predrift Position of the Continents, *Geological Society of America Bulletin*, 82, 1285-
978 1292.

979 Mazza, S. E., E. Gazel, E. A. Johnson, M. Bizimis, R. McAleer, and C. B. Biryol (2017), Post-
980 rift magmatic evolution of the eastern North American “passive-aggressive” margin,
981 *Geochemistry, Geophysics, Geosystems*, 18(1), 3-22.

982 Mazza, S. E., E. Gazel, M. Bizimis, R. Moucha, P. Béguelin, E. A. Johnson, R. J. McAleer, and
983 A. V. Sobolev (2019), Sampling the volatile-rich transition zone beneath Bermuda, *Nature*,
984 569(7756), 398.

985 McHone, J. G. (1978), Distribution, orientations, and ages of mafic dikes in central New
986 England, *Geological Society of America Bulletin*, 89(11), 1645-1655.

987 McHone, G. (1996), Broad-terrane Jurassic flood basalts across northeastern North America,
988 *Geology*, 24, 319-322.

989 McHone, J. G. (2000), Non-plume magmatism and rifting during the opening of the central
990 Atlantic Ocean, *Tectonophysics*, 316, 287-296.

991 McKenzie, D., and R. O’Nions (1991), Partial Melt Distributions From Inversion Of Rare-Earth
992 Element Concentrations, *Journal of Petrology*, 32, 1021.

993 Merle, R., A. Marzoli, H. Bertrand, L. Reisberg, C. Verati, C. Zimmermann, M. Chiaradia, and
994 G. Bellieni (2011), $^{40}\text{Ar}/^{39}\text{Ar}$ ages and Sr-Nd-Pb-Os geochemistry of CAMP tholeiites from
995 Western Maranhao basin (NE Brazil), *Lithos*, 122, 137-151.

996 Merle, R., A. Marzoli, L. Reisberg, H. Bertrand, A. Nemchin, M. Chiaradia, S. Callegaro, F.
997 Jourdan, G. Bellieni, D. Kontak, J. Puffer, and J.G. McHone (2014), Sr, Nd, Pb and Os Isotope
998 Systematics of CAMP Tholeiites from Eastern North America (ENA): Evidence of a
999 Subduction-enriched Mantle Source, *Journal of Petrology*, 55(1), 133-180.

1000 Morgan, P. (1983), Constraints on rift thermal processes from heat flow and uplift,
1001 *Tectonophysics*, 94(1), 277-298.

1002 Münker, C., S. Weyer, E. Scherer, and K. Mezger (2001), Separation of high field strength
1003 elements (Nb, Ta, Zr, Hf) and Lu from rock samples for MC-ICPMS measurements, *Geochem.*
1004 *Geophys. Geosyst.*, 2(12), doi: 10.1029/2001GC000183.

1005 Nehring, F., S.F. Foley, and P. Hölttä (2010), Trace element partitioning in the granulite facies,
1006 *Contrib. Mineral. Petrol.*, 159, 493-519.

1007 Nomade, S., K. Knight, E. Beutel, P. Renne, C. Verati, G. Féraud, A. Marzoli, N. Youbi, and H.
1008 Bertrand (2007), Chronology of the Central Atlantic Magmatic Province: Implications for the
1009 Central Atlantic rifting processes and the Triassic-Jurassic biotic crisis, *Palaeogeography,*
1010 *Palaeoclimatology, Palaeoecology*, 244(1), 326-344.

1011 Oyarzun, R., M. Doblas, J. López-Ruiz, and J. M. Cebriá (1997), Opening of the central Atlantic
1012 and asymmetric mantle upwelling phenomena: implications for long-lived magmatism in western
1013 North Africa and Europe, *Geology*, 25(8), 727-730.

1014 Papezik, V., J. D. Greenough, J. A. Colwell, and T. J. Mallinson (1988), North Mountain basalt
1015 from Digby, Nova Scotia: models for a fissure eruption from stratigraphy and petrochemistry,
1016 *Canadian Journal of Earth Sciences*, 25(1), 74-83.

1017 Pe-Piper, G., and D. J. W. Piper (1999), Were Jurassic tholeiitic lavas originally widespread in
1018 southeastern Canada?: a test of the broad terrane hypothesis, *Canadian Journal of Earth*
1019 *Sciences*, 36(9), 1509-1516.

1020 Pegram, W. J. (1990), Development of continental lithospheric mantle as reflected in the
1021 chemistry of the Mesozoic Appalachian tholeiites, USA, *Earth and Planetary Science Letters*,
1022 97(3), 316-331.

1023 Pettingill, H. S., A. Sinha, and M. Tatsumoto (1984), Age and origin of anorthosites,
1024 charnockites, and granulites in the central Virginia Blue Ridge: Nd and Sr isotopic evidence,
1025 *Contributions to Mineralogy and Petrology*, 85(3), 279-291.

1026 Plank, T., and C. H. Langmuir (1998), The chemical composition of subducting sediment and its
1027 consequences for the crust and mantle, *Chemical geology*, 145(3), 325-394.

1028 Puffer, J. (1992), Eastern North American flood basalts in the context of the incipient breakup of
1029 Pangea, , In *Eastern North American Mesozoic Magmatism*, Eds. Puffer, J.H. and P.C. Ragland,
1030 *Special Papers-Geological Society of America*, v. 268, 95.

1031 Puffer, J. (2001), Contrasting high field strength element contents of continental flood basalts
1032 from plume versus reactivated-arc sources, *Geology*, 29(8), 675-678.

- 1033 Puffer, J. H. (2003), A reactivated back-arc source for CAMP magma, *Geophysical Monograph*
1034 *Series, 136*, 151-162.
- 1035 Puffer, J., D. Hurlbise, F. Geiger, and P. Lechler (1981), Chemical composition and
1036 stratigraphic correlation of the Mesozoic basalt units of the Newark Basin, New Jersey, and the
1037 Hartford Basin, Connecticut, *Geological Society of America Bulletin*, 92, 515-553.
- 1038 Ragland, P., L. Cummins, and J. Arthur (1992), Compositional patterns for early Mesozoic
1039 diabases from South Carolina to central Virginia, In *Eastern North American Mesozoic*
1040 *Magmatism*, Eds. Puffer, J.H. and P.C. Ragland, *Special Papers-Geological Society of America*,
1041 v. 268, 309.
- 1042 Reinemund, J. A. (1955), *Geology of the Deep River coal field, North Carolina*, Geological
1043 Survey Professional Paper 246, U.S. Government Printing Office, Washington, D.C.
- 1044 Rey, P. F. (2015), The geodynamics of mantle melting, *Geology*, 43(4), 367-368.
- 1045 Ruiz-Martínez, V. C., T. H. Torsvik, D. J. J. van Hinsbergen, and C. Gaina (2012), Earth at
1046 200Ma: Global palaeogeography refined from CAMP palaeomagnetic data, *Earth and Planetary*
1047 *Science Letters*, 331, 67-79.
- 1048 Salters, V. J. M., and S. R. Hart (1989), The Hafnium Paradox and the Role of Garnet in the
1049 Source of Mid-Ocean-Ridge Basalts, *Nature*, 342(6248), 420-422.
- 1050 Salters, V. J., and A. Stracke (2004), Composition of the depleted mantle, *Geochemistry*,
1051 *Geophysics, Geosystems*, 5(5), doi: 10.1029/2003GC000597.

1052 Salters, V. J., J. Blichert-Toft, Z. Fekiacova, A. Sachi-Kocher, and M. Bizimis (2006), Isotope
1053 and trace element evidence for depleted lithosphere in the source of enriched Ko'olau basalts,
1054 *Contributions to Mineralogy and Petrology*, 151(3), 297-312.

1055 Salters, V. J., S. Mallick, S. R. Hart, C. E. Langmuir, and A. Stracke (2011), Domains of
1056 depleted mantle: New evidence from hafnium and neodymium isotopes, *Geochemistry,*
1057 *Geophysics, Geosystems*, 12(8), doi: 10.1029/2011GC003617.

1058 Saunders, A. D., S. M. Jones, L. A. Morgan, K. L. Pierce, M. Widdowson, and Y. G. Xu (2007),
1059 Regional uplift associated with continental large igneous provinces; the roles of mantle plumes
1060 and the lithosphere, *Chemical Geology*, 241(3-4), 282-318.

1061 Schmitz, M. D., J. D. Vervoort, S. A. Bowring, and P. J. Patchett (2004), Decoupling of the Lu-
1062 Hf and Sm-Nd isotope systems during the evolution of granulitic lower crust beneath southern
1063 Africa, *Geology*, 32(5), 405-408.

1064 Sebai, A., G. Feraud, H. Bertrand, and J. Hanes (1991), $^{40}\text{Ar}/^{39}\text{Ar}$ dating and geochemistry of
1065 tholeiitic magmatism related to the early opening of the Central Atlantic Rift, *Earth and*
1066 *Planetary Science Letters*, 104(2), 455-472.

1067 Sengör, A., and K. Burke (1978), Relative timing of rifting and volcanism on Earth and its
1068 tectonic implications, *Geophysical Research Letters*, 5(6), 419-421.

1069 Shaw, J., J. Baker, A. Kent, K. Ibrahim, and M. Menzies (2007), The geochemistry of the
1070 Arabian lithospheric mantle—a source for intraplate volcanism?, *Journal of Petrology*, 48(8),
1071 1495-1512.

1072 Shellnutt, J. G., J. Dostal, and M.-W. Yeh (2018), Mantle source heterogeneity of the Early
1073 Jurassic basalt of eastern North America, *International Journal of Earth Sciences*, 107(3), 1033-
1074 1058.

1075 Sinha, A., J. Hogan, and J. Parks (1996), Lead Isotope Mapping of Crustal Reservoirs Within the
1076 Grenville Supertereane: I. Central and Southern Appalachians, *Geophysical Monograph-*
1077 *American Geophysical Union*, 95, 293-306.

1078 Sobolev, S. V., A. V. Sobolev, D. V. Kuzmin, N. A. Krivolutsкая, A. G. Petrunin, N. T. Arndt,
1079 V. A. Radko, and Y. R. Vasiliev (2011), Linking mantle plumes, large igneous provinces and
1080 environmental catastrophes, *Nature*, 477(7364), 312-316.

1081 Söderlund, U., P. J. Patchett, J. D. Vervoort, and C. E. Isachsen (2004), The ^{176}Lu decay constant
1082 determined by Lu–Hf and U–Pb isotope systematics of Precambrian mafic intrusions, *Earth and*
1083 *Planetary Science Letters*, 219(3-4), 311-324.

1084 Spera, F. J., and W. A. Bohrson (2001), Energy-constrained open-system magmatic processes I:
1085 General model and energy-constrained assimilation and fractional crystallization (EC-AFC)
1086 formulation, *Journal of Petrology*, 42(5), 999-1018.

1087 Staudigel, H., T. Plank, B. White, and H. U. Schmincke (1996), Geochemical fluxes during
1088 seafloor alteration of the basaltic upper oceanic crust: DSDP Sites 417 and 418, *Subduction: top*
1089 *to bottom*, 96, 19-38.

1090 Stracke, A., M. Bizimis, and V. J. M. Salters (2003), Recycling oceanic crust: Quantitative
1091 constraints, *Geochemistry, Geophysics, Geosystems*, 4(3), 8003.

1092 Taylor, S. R., and S. M. McLennan (1995), The geochemical evolution of the continental crust,
1093 *Reviews of Geophysics*, 33(2), 241-265.

1094 Tollo, R., and D. Gottfried (1992), Petrochemistry of Jurassic basalt from eight cores, Newark
1095 basin, New Jersey, In *Eastern North American Mesozoic Magmatism*, Eds. Puffer, J.H. and P.C.
1096 Ragland, *Special Papers-Geological Society of America*, v. 268, 233.

1097 Verati, C., H. Bertrand, and G. Féraud (2005), The farthest record of the Central Atlantic
1098 Magmatic Province into West Africa craton: Precise $^{40}\text{Ar}/^{39}\text{Ar}$ dating and geochemistry of
1099 Taoudenni basin intrusives (northern Mali), *Earth and Planetary Science Letters*, 235(1), 391-
1100 407.

1101 Verati, C., C. Rapaille, G. Féraud, A. Marzoli, H. Bertrand, and N. Youbi (2007), $^{40}\text{Ar}/^{39}\text{Ar}$ ages
1102 and duration of the Central Atlantic Magmatic Province volcanism in Morocco and Portugal and
1103 its relation to the Triassic-Jurassic boundary, *Palaeogeography, Palaeoclimatology,*
1104 *Palaeoecology*, 244(1), 308-325.

1105 Vervoort, J. D., P. J. Patchett, J. Blichert-Toft, and F. Albarede (1999), Relationships between
1106 Lu-Hf and Sm-Nd isotopic systems in the global sedimentary system, *Earth and Planetary*
1107 *Science Letters*, 168(1-2), 79-99.

1108 Vervoort, J. D., P. J. Patchett, F. Albarede, J. Blichert-Toft, R. Rudnick, and H. Downes (2000),
1109 Hf-Nd isotopic evolution of the lower crust, *Earth and Planetary Science Letters*, 181(1-2), 115-
1110 129.

1111 Vervoort, J. D., T. Plank, and J. Prytulak (2011), The Hf-Nd isotopic composition of marine
1112 sediments, *Geochimica Et Cosmochimica Acta*, 75, 5903-5926.

1113 Wedepohl, K. H. (1995), The composition of the continental crust, *Geochimica et cosmochimica*
1114 *Acta*, 59(7), 1217-1232.

1115 Weigand, P. W., and P. C. Ragland (1970), Geochemistry of Mesozoic dolerite dikes from
1116 eastern North America, *Contributions to Mineralogy and Petrology*, 29(3), 195-214.

1117 Whalen, L., E. Gazel, C. Vidito, J. Puffer, M. Bizimis, W. Henika, and M. J. Caddick (2015),
1118 Supercontinental inheritance and its influence on supercontinental breakup: The Central Atlantic
1119 Magmatic Province and the breakup of Pangea, *Geochemistry Geophysics Geosystems*, 16(10),
1120 3532-3554.

1121 White, R. S., and D. P. McKenzie (1989), Volcanism at Rifts, *Scientific American*, 261(1), 62-
1122 71.

1123 Willbold, M., and A. Stracke (2006), Trace element composition of mantle end-members:
1124 Implications for recycling of oceanic and upper and lower continental crust, *Geochem. Geophys.*
1125 *Geosyst.*, 7(4), doi: 10.1029/2005GC001005.

1126 Wilson, J. T. (1966), Did the Atlantic close and then re-open?, *Nature*, 211, 676-681.

1127 Wilson, M. (1997), Thermal evolution of the Central Atlantic passive margins: continental
1128 break-up above a Mesozoic super-plume, *Journal of the Geological Society*, 154(3), 491-495.

1129 Wittig, N., J. A. Baker, and H. Downes (2007), U–Th–Pb and Lu–Hf isotopic constraints on the
1130 evolution of sub-continental lithospheric mantle, French Massif Central, *Geochimica et*
1131 *Cosmochimica Acta*, 71(5), 1290-1311.

1132 Wittig, N., D. G. Pearson, S. Duggen, J. A. Baker, and K. Hoernle (2010), Tracing the
1133 metasomatic and magmatic evolution of continental mantle roots with Sr, Nd, Hf and and Pb
1134 isotopes: A case study of Middle Atlas (Morocco) peridotite xenoliths, *Geochimica Et*
1135 *Cosmochimica Acta*, 74(4), 1417-1435.

1136 Woodhead, J. D., and C. W. Devey (1993), Geochemistry of the Pitcairn seamounts, I: source
1137 character and temporal trends, *Earth and Planetary Science Letters*, 116(1-4), 81-99.

1138 Workman, R. K., and S. R. Hart (2005), Major and trace element composition of the depleted
1139 MORB mantle (DMM), *Earth and Planetary Science Letters*, 231, 53-72.

1140 Workman, R. K., S. R. Hart, M. Jackson, M. Regelous, K. Farley, J. Blusztajn, M. Kurz, and H.
1141 Staudigel (2004), Recycled metasomatized lithosphere as the origin of the Enriched Mantle II
1142 (EM2) end-member: Evidence from the Samoan Volcanic Chain, *Geochemistry, Geophysics,*
1143 *Geosystems*, 5(4), doi: 10.1029/2003GC000623.

1144 Wysoczanski, R., J. Gamble, P. Kyle, and M. Thirlwall (1995), The petrology of lower crustal
1145 xenoliths from the Executive Committee Range, Marie Byrd Land volcanic province, West
1146 Antarctica, *Lithos*, 36(3-4), 185-201.

1147 Zartman, R. E., P. D. Kempton, J. B. Paces, H. Downes, I. S. Williams, G. Dobosi, and K. Futral
1148 (2013), Lower-crustal xenoliths from Jurassic kimberlite diatremes, Upper Michigan (USA):
1149 Evidence for Proterozoic Orogenesis and plume magmatism in the lower crust of the Southern
1150 Superior Province, *Journal of Petrology*, 54, 575-608.

1151 Zhao, S., and W. Guo (2019), Crustal Structure of Eastern North Carolina: Piedmont and Coastal
1152 Plain, *Bulletin of the Seismological Society of America*, 109(6), 2288-2304.

1153

1154 **FIGURE CAPTIONS**

1155 Figure 1. Tectonic reconstruction of the central Atlantic region around the time of CAMP
1156 emplacement, with Southern and Northern ENA, Morocco, and Sierra Leone sample locations
1157 for this study indicated. Lines and fields in red and blue show the locations of CAMP intrusions
1158 and lava flows, as indicated in the legend (after Deckart et al., 2005, Marzoli et al., 2018).
1159 Indicated groupings within CAMP refer to magma categories defined by Marzoli et al. (2018).

1160 Figure 2. Age-corrected isotope results for samples analyzed in this study, with comparative
1161 values from the literature, for **a.** $\epsilon_{\text{Hf } 201\text{Ma}}$ vs. $\epsilon_{\text{Nd } 201\text{Ma}}$, **b.** $\epsilon_{\text{Hf } 201\text{Ma}}$ vs. $^{206}\text{Pb}/^{204}\text{Pb}_{201\text{Ma}}$, and **c.**
1162 $^{207}\text{Pb}/^{204}\text{Pb}_{201\text{Ma}}$ vs. $^{206}\text{Pb}/^{204}\text{Pb}_{201\text{Ma}}$. Lead and $\epsilon_{\text{Nd } 201\text{Ma}}$ isotope data for samples in this study are
1163 from Callegaro et al. (2013, 2017) and Merle et al. (2014). Other literature data for CAMP are
1164 from Callegaro et al. (2013, 2014, 2017), Deckart et al. (2005), Jourdan et al. (2003), Marzoli et
1165 al. (2019), Merle et al. (2011, 2014), and Whalen et al. (2015), with regional groups defined after
1166 Whalen et al. (2015). End members are shown as black squares, with values as in Table S1 and
1167 described in the text; “GLOSS” refers to global average subducted sediment after Plank and
1168 Langmuir (1998) and Chauvel et al. (2008), aged 170 Ma to represent Paleozoic subducted
1169 sediments (that is, assuming a subduction recycling age of ~370 Ma sampled by CAMP melting
1170 at ~200 Ma, after Callegaro et al. (2013) and Whalen et al. (2015)), “UCC” refers to the average
1171 composition of upper continental crust from the Carolina terrane, “Mafic LCC” and
1172 “Intermediate LCC” refer to Proterozoic mafic and intermediate-SiO₂ lower continental crust

1173 compositions, as described in the text and Table S2, and the “Geochron” line shows the
1174 composition of the geochron corrected to an age of 201 Ma. Also shown for reference are the ϵ_{Hf}
1175 vs. ϵ_{Nd} mantle array (Vervoort et al., 2011), the field of MORB (Chauvel et al., 2008), the field
1176 of Hawaiian lavas (Blichert-Toft et al., 1999), the global seawater array and the field of
1177 ferromanganese nodules (after Albarede et al., 1998), average marine sediments from Chauvel et
1178 al. (2014) and Plank and Langmuir (1998), and the field of Karoo LIP basalts (Jourdan et al.,
1179 2007), which exhibits a shallow sloping trend similar to Hawaiian basalts and our ENA CAMP
1180 array. The composition of average Atlantic OIB is after Marzoli et al. (2019) and references
1181 therein, e.g. Cape Verde data from Holm et al. (2006) and Canary Islands data from Klügel et al.
1182 (2017). Data sets and compositions unrelated to CAMP are plotted for reference and have not
1183 been age-corrected, except where indicated in the text or data tables. End-member, age-corrected
1184 isotopic compositions for EM-1, EM-2, and DMM were calculated using the compositions
1185 shown in Table S1.

1186 Figure 3. **a.** $\epsilon_{\text{Hf}} 201\text{Ma}$ vs. $\epsilon_{\text{Nd}} 201\text{Ma}$ and **b.** $\epsilon_{\text{Hf}} 201\text{Ma}$ vs. $^{206}\text{Pb}/^{204}\text{Pb}_{201\text{Ma}}$ diagrams for samples from
1187 this study, showing calculated EC-AFC trajectories after Bohrson and Spera (2001) and Spera
1188 and Bohrson (2001), as described in the text and using values from Table S1. Trajectories are
1189 shown for a parent basalt composition similar to sample CS49, which has the most incompatible
1190 element depleted composition based on radiogenic isotope compositions (yellow star; Table 2),
1191 with hypothesized compositions for several upper and lower continental crust assimilants
1192 described in the text and shown in Table S2. The assimilants shown are 1) averaged Carolina
1193 terrane upper continental crust (“Carolina UCC”); 2) a Proterozoic lower crustal mafic granulite
1194 (“Mafic LCC”); and 3) an intermediate lower continental granulite with a hypothesized
1195 $^{206}\text{Pb}/^{204}\text{Pb}_{201\text{Ma}}$ ratio of 17.3, after the discussion in the text (“Intermediate LCC”). Upper

1196 continental crust was calculated using mean compositions of measured Carolina terrane crustal
1197 rocks from Pettingill et al. (1984) and Sinha et al. (1996) and the data compilation of Whalen et
1198 al. (2015). Carolina terrane crustal data set lacks hafnium isotope measurements, so UCC ϵ_{Hf}
1199 $_{201\text{Ma}}$ values were then calculated assuming a relationship with $\epsilon_{\text{Nd } 201\text{Ma}}$ along the terrestrial array
1200 (Vervoort et al., 1999) (Table S1). The Proterozoic mafic granulite shown has elevated Lu/Hf
1201 ratios, similar to average mafic xenoliths from Michigan (Zartman et al., 2013) and
1202 representative of mafic LCC with decoupled ϵ_{Hf} and ϵ_{Nd} . In panel (b), we additionally test mafic
1203 LCC with an alternative Pb isotope composition more closely resembling comparable mafic
1204 granulite xenoliths from Markt, South Africa (Huang et al., 1995) (“Markt LCC”). Intermediate
1205 granulites may have isotopic signatures that record higher time-integrated incompatible element
1206 concentrations than mafic basement (i.e., less radiogenic $^{143}\text{Nd}/^{144}\text{Nd}$ and $^{176}\text{Hf}/^{177}\text{Hf}$ ratios), so
1207 the intermediate LCC composition has a relatively incompatible element-enriched composition
1208 within the range of xenolith measurements by Schmitz et al. (2004). For our intermediate-SiO₂
1209 granulite composition, we also determined partitioning behavior using mineral modes similar to
1210 the intermediate-SiO₂ xenolith sampled by Zartman et al (2013). Tickmarks indicate the
1211 percentage of crustal assimilant added to the magma, up to a maximum of 10% addition. All
1212 other symbols and lines as in Figure 2.

1213 Figure 4. Ternary mixing diagrams for partial melts of DMM, EM-1, and EM-2 sources, as
1214 defined in Table S1 and the text, for a. $\epsilon_{\text{Hf } 201\text{Ma}}$ vs. $\epsilon_{\text{Nd } 201\text{Ma}}$, b. $\epsilon_{\text{Hf } 201\text{Ma}}$ vs. $^{206}\text{Pb}/^{204}\text{Pb}_{201\text{Ma}}$, and
1215 c. $^{207}\text{Pb}/^{204}\text{Pb}_{201\text{Ma}}$ vs. $^{206}\text{Pb}/^{204}\text{Pb}_{201\text{Ma}}$. Mixing lines are plotted in 10% increments; symbols,
1216 lines, and mixing reservoirs as in Figure 2. Mantle reservoirs used for the mixing calculations
1217 use relatively recent estimates for the isotopic composition of enriched mantle sources (e.g.,
1218 Jackson and Dasgupta, 2008; Jackson et al., 2007), resulting in different values than prior

1219 studies; however, the results confirm that mixing of these reservoirs fails to explain southern
1220 ENA CAMP (Callegaro et al., 2013). More recent research (e.g., Marzoli et al., 2019) suggests
1221 that CAMP asthenosphere was in fact less depleted than global DMM and may more closely
1222 resemble the PREMA reservoir (Zindler and Hart, 1986), but our mixing trajectories show that
1223 the enriched melting end-members are mainly responsible for the observed mismatch, not the
1224 depleted end-member.

1225 Figure 5. Ternary mixing diagrams for solid DMM, EM-1, and EM-2 source reservoirs, as
1226 defined in Table S1 and the text, for a. $\epsilon_{\text{Hf } 201\text{Ma}}$ vs. $\epsilon_{\text{Nd } 201\text{Ma}}$, b. $\epsilon_{\text{Hf } 201\text{Ma}}$ vs. $^{206}\text{Pb}/^{204}\text{Pb}_{201\text{Ma}}$, and
1227 c. $^{207}\text{Pb}/^{204}\text{Pb}_{201\text{Ma}}$ vs. $^{206}\text{Pb}/^{204}\text{Pb}_{201\text{Ma}}$. Mixing lines are plotted in 10% increments; symbols,
1228 lines, and mixing reservoirs as in Figure 2.

1229 Figure 6. Ternary mixing diagrams for DMM melts, average Carolina terrane continental crust,
1230 and average subducted pelagic marine sediments (GLOSS), as defined in Table S1 and the text,
1231 for a. $\epsilon_{\text{Hf } 201\text{Ma}}$ vs. $\epsilon_{\text{Nd } 201\text{Ma}}$, b. $\epsilon_{\text{Hf } 201\text{Ma}}$ vs. $^{206}\text{Pb}/^{204}\text{Pb}_{201\text{Ma}}$, and c. $^{207}\text{Pb}/^{204}\text{Pb}_{201\text{Ma}}$ vs.
1232 $^{206}\text{Pb}/^{204}\text{Pb}_{201\text{Ma}}$. Mixing lines are plotted in 10% increments; other symbols, lines, and mixing
1233 reservoirs as in Figure 2.

1234 Figure 7. Isotope diagrams showing results of isotopic evolution and partial melting calculations
1235 for modified mantle wedge, for a. $\epsilon_{\text{Hf } 201\text{Ma}}$ vs. $\epsilon_{\text{Nd } 201\text{Ma}}$, b. $\epsilon_{\text{Hf } 201\text{Ma}}$ vs. $^{206}\text{Pb}/^{204}\text{Pb}_{201\text{Ma}}$, and c.
1236 $^{207}\text{Pb}/^{204}\text{Pb}_{201\text{Ma}}$ vs. $^{206}\text{Pb}/^{204}\text{Pb}_{201\text{Ma}}$ and with symbols and lines as in Figure 2. The trajectories
1237 shown indicate calculated mantle compositions for a crustal recycling subduction and
1238 metasomatism age of 370 Ma and subsequent mantle melting at 201 Ma. Blue solid lines indicate
1239 mantle compositions when metasomatized by a mixture of fluid derived from altered oceanic
1240 crust (AOC) and fluid derived from subducted global oceanic sediment; “% Sed Fluid” labels

1241 indicate the percentage of sediment-derived fluid in the metasomatizing fluid mixture. Red solid
1242 lines indicate the same, but for AOC-derived fluid and sediment-derived partial melts (with
1243 corresponding “% Sed Melt” labels). Dashed lines and associated labels indicate the amount of
1244 fluid added to the mantle during metasomatism up to 10% addition, as a mass fraction relative to
1245 the initial mantle material (0.01 to 0.10). We note that all fractions of added fluid from 1-10%
1246 addition are compressed into a single narrow zone in panel **c** and so are not labeled. See Table S4
1247 for additional modeling details.

1248 Figure 8. Diagrams showing mixing trajectories between recycled continental crustal rocks and
1249 partial melts of modified, metasomatized mantle, for **a.** $\epsilon_{\text{Hf } 201\text{Ma}}$ vs. $\epsilon_{\text{Nd } 201\text{Ma}}$, **b.** $\epsilon_{\text{Hf } 201\text{Ma}}$ vs.
1250 $^{206}\text{Pb}/^{204}\text{Pb}_{201\text{Ma}}$, and **c.** $^{207}\text{Pb}/^{204}\text{Pb}_{201\text{Ma}}$ vs. $^{206}\text{Pb}/^{204}\text{Pb}_{201\text{Ma}}$ and with mixing lines in 10%
1251 increments and all other symbols as in Figure 2. The “modified mantle” mixing end member is a
1252 calculated 6% batch melt of mantle metasomatized using the methods described in the text and
1253 shown in Figure 7 and Table S4. The example case shown is for mantle modified by 7% addition
1254 of a fluid derived 25% from AOC and 75% from subducted sediments, with a 370 Ma recycling
1255 age and 201 Ma melting age. The UCC composition shown is local Carolina terrane, and the
1256 LCC composition is the “Markt mafic granulite” composition, both from Table S1.

Figure 1.

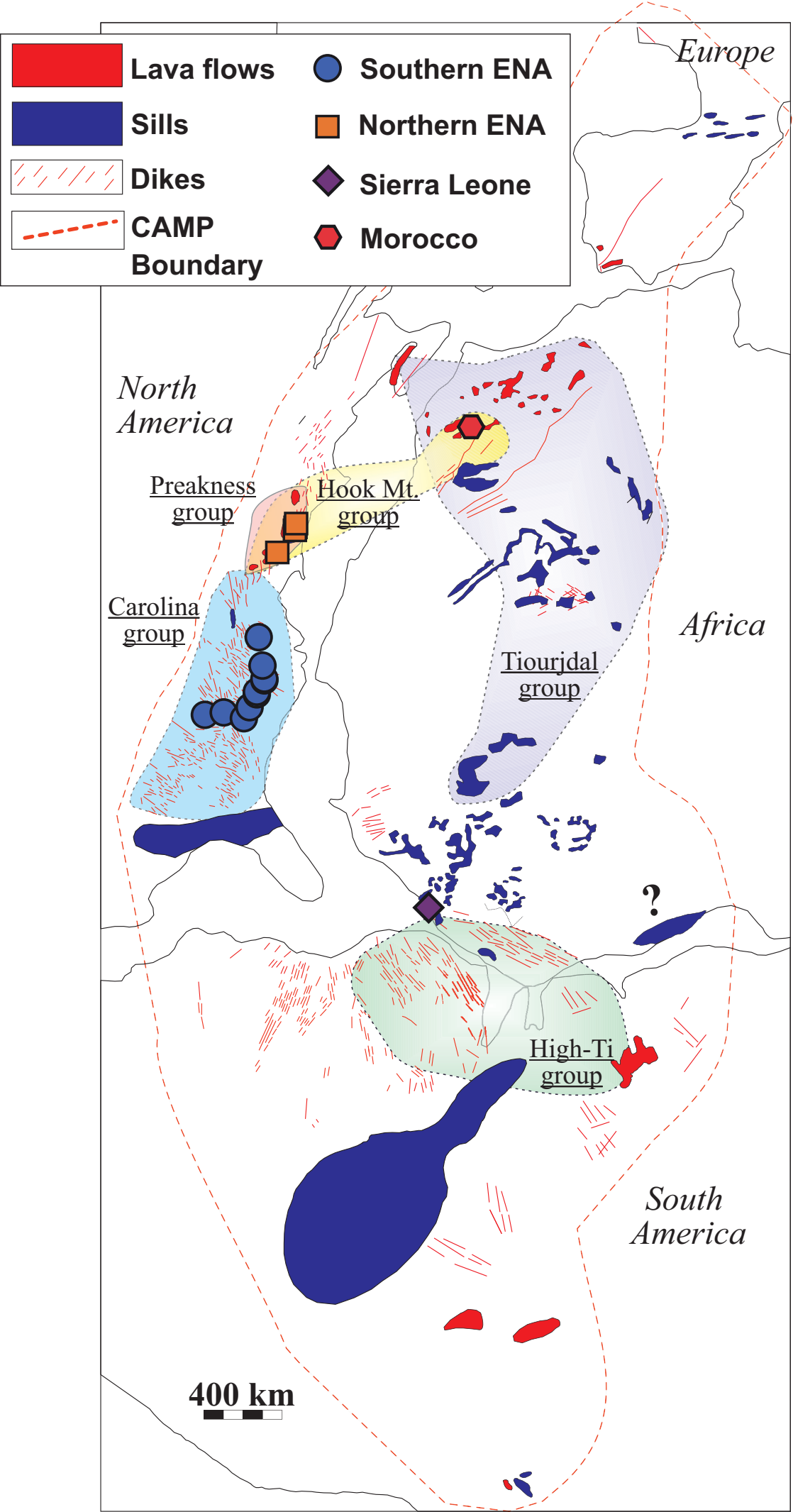


Figure 2.

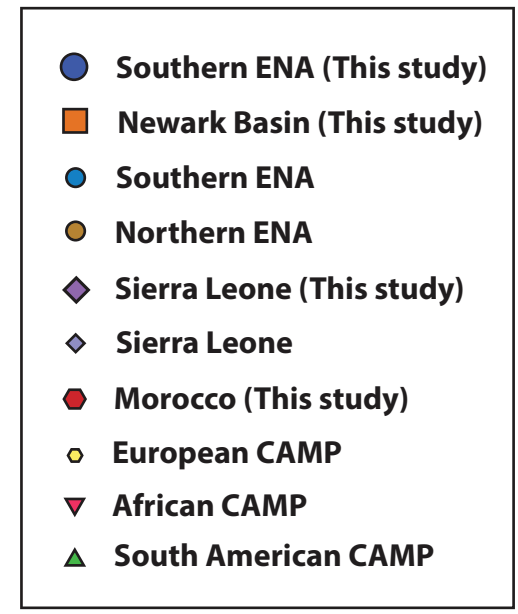
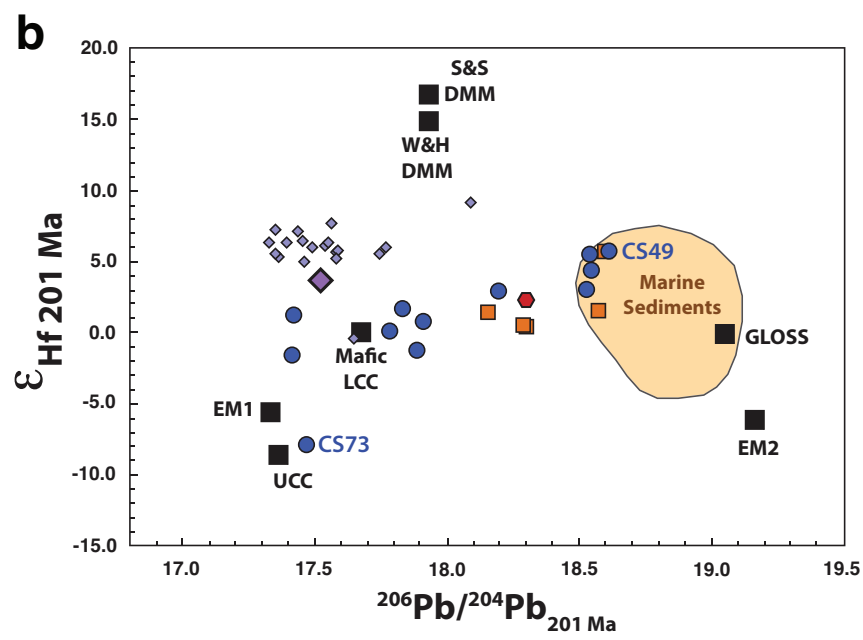
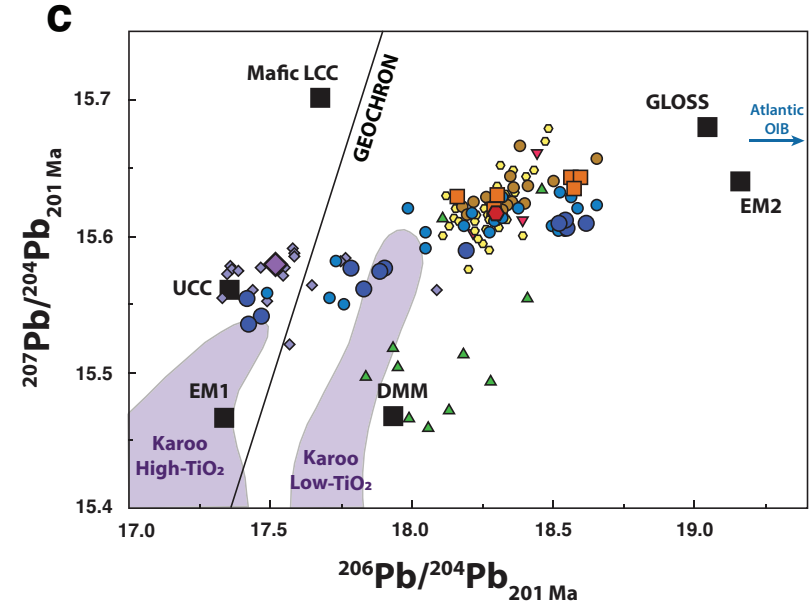
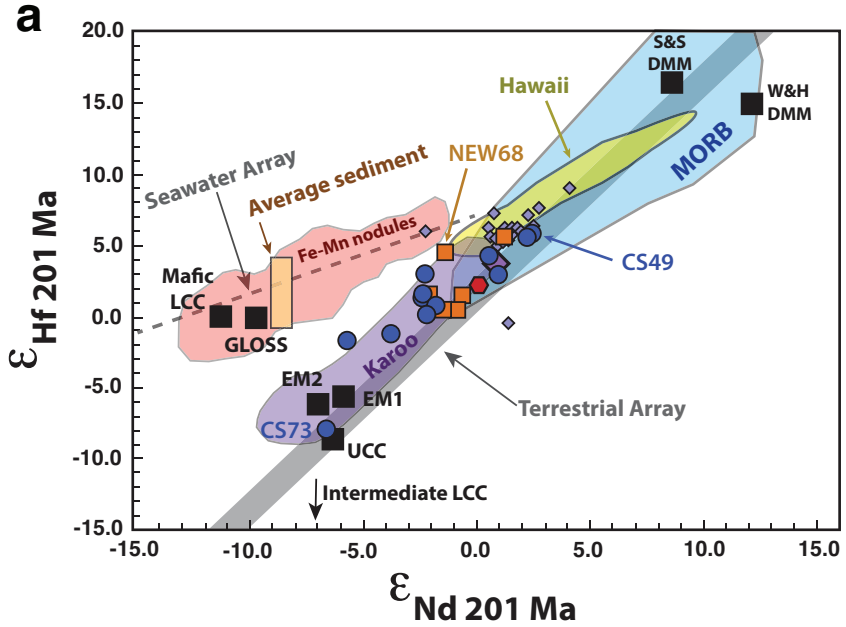


Figure 3.

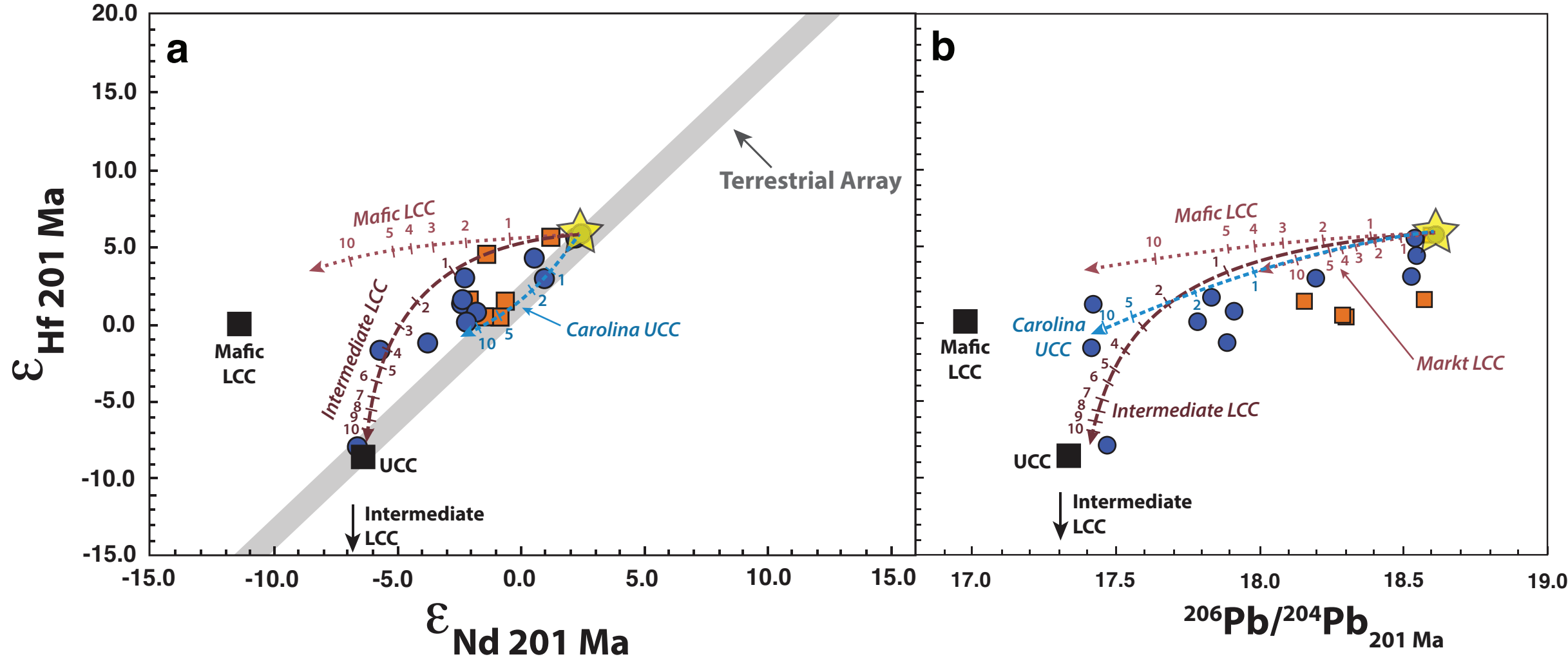


Figure 4.

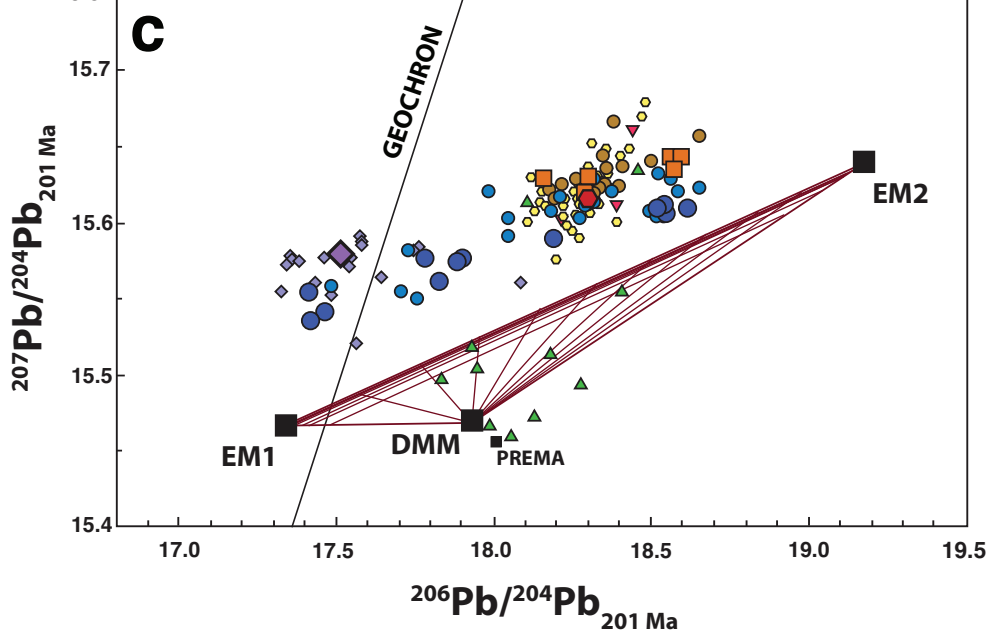
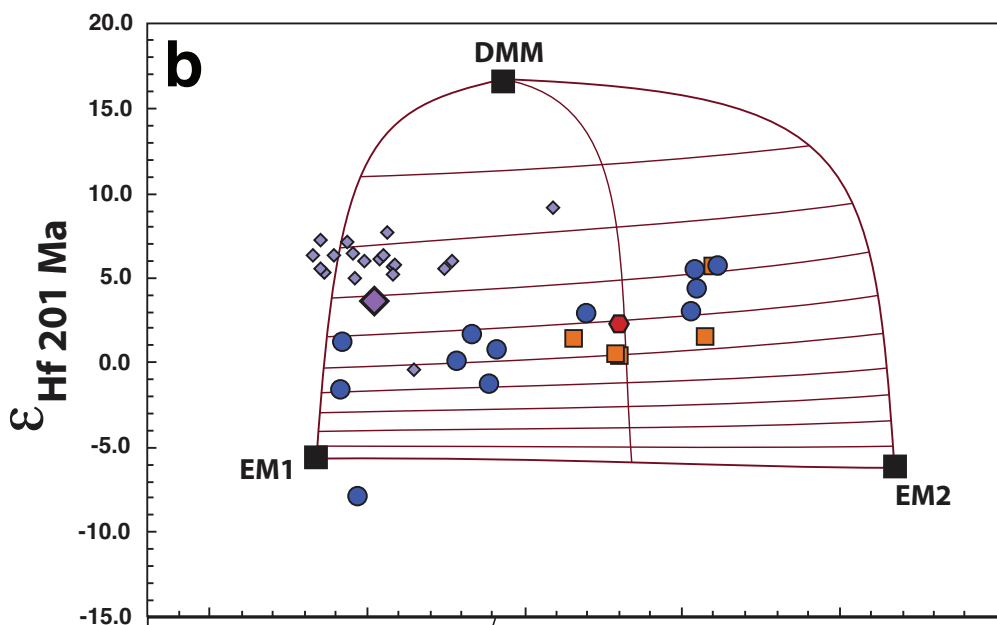
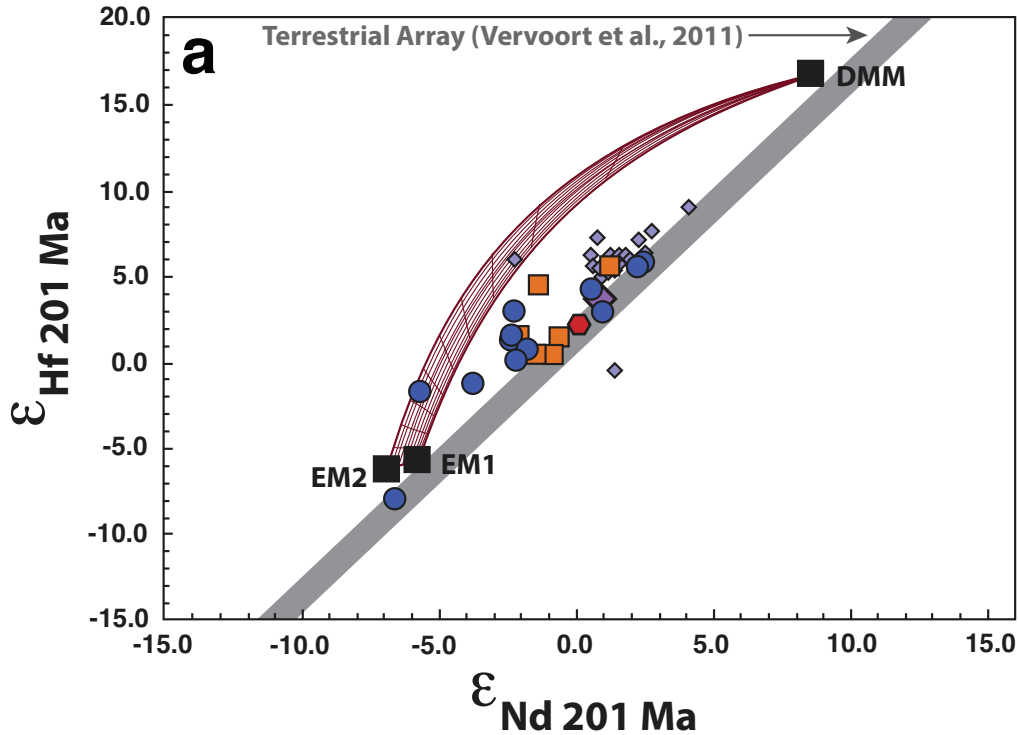


Figure 5.

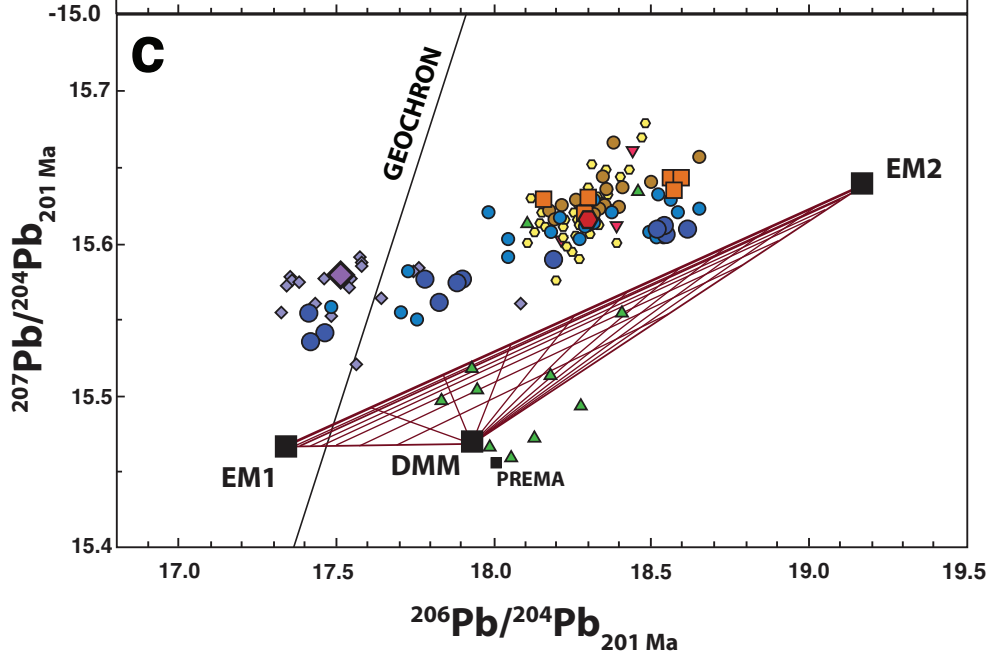
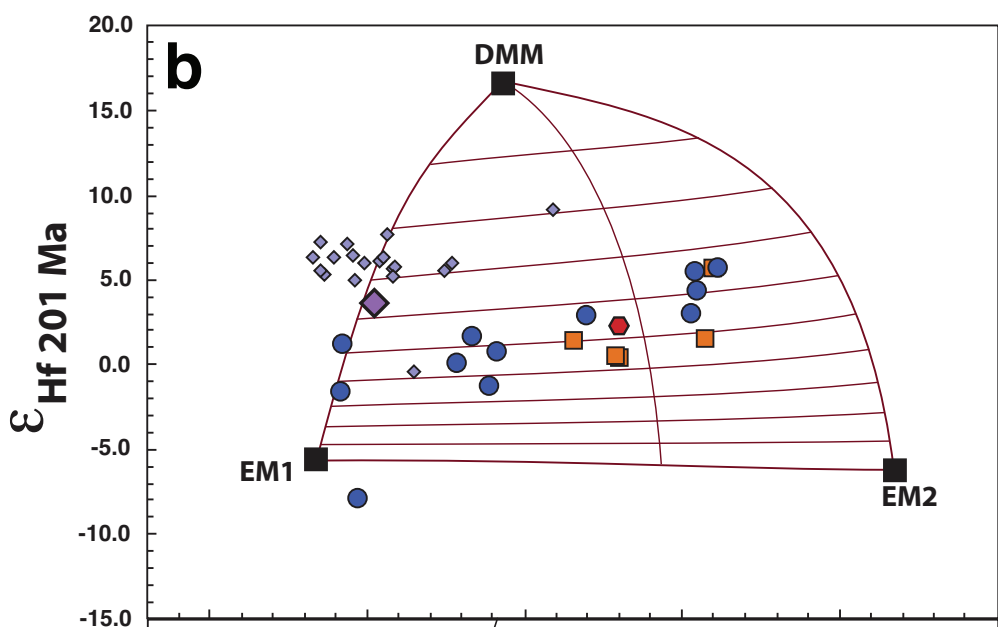
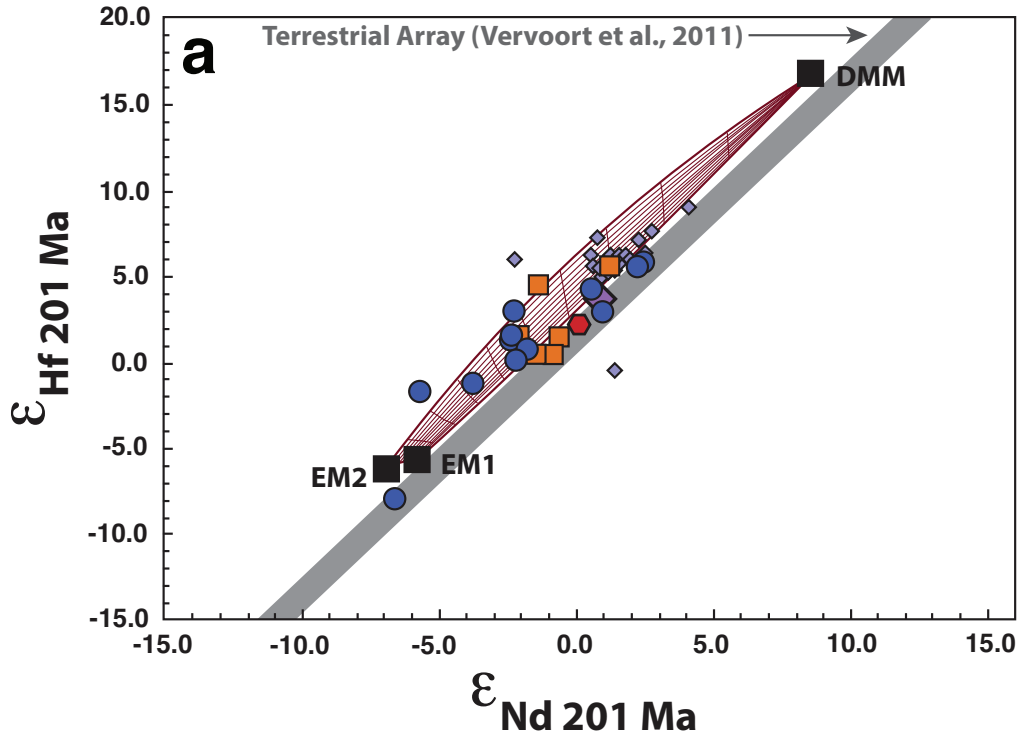


Figure 6.

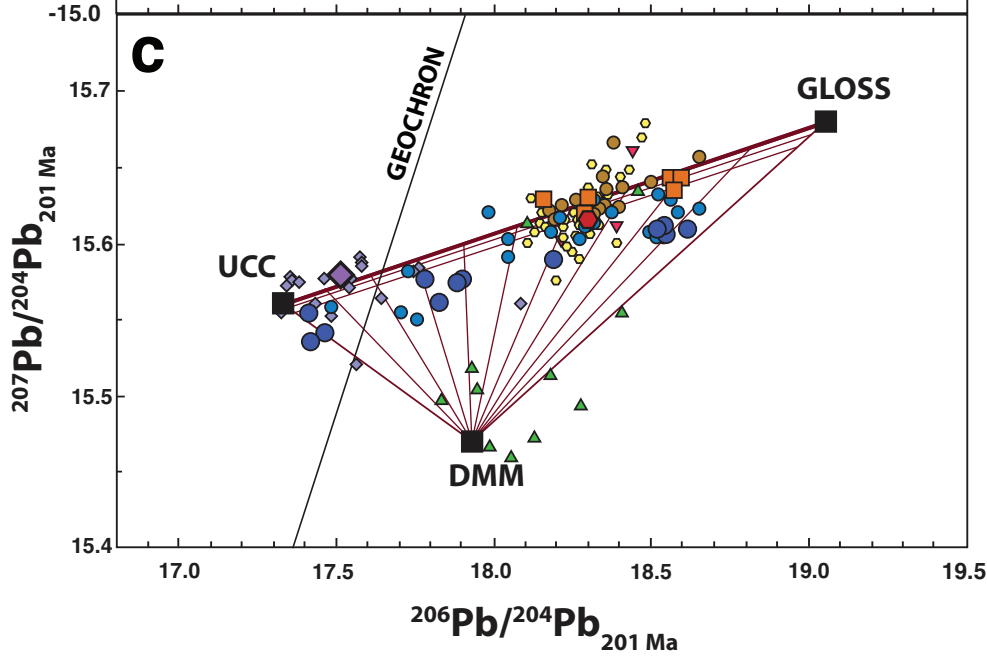
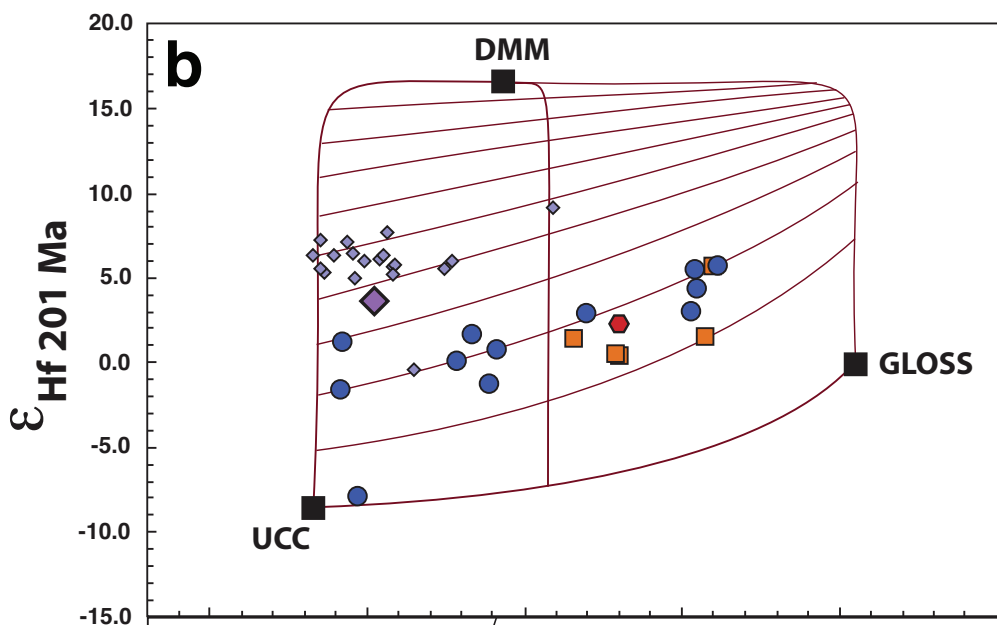
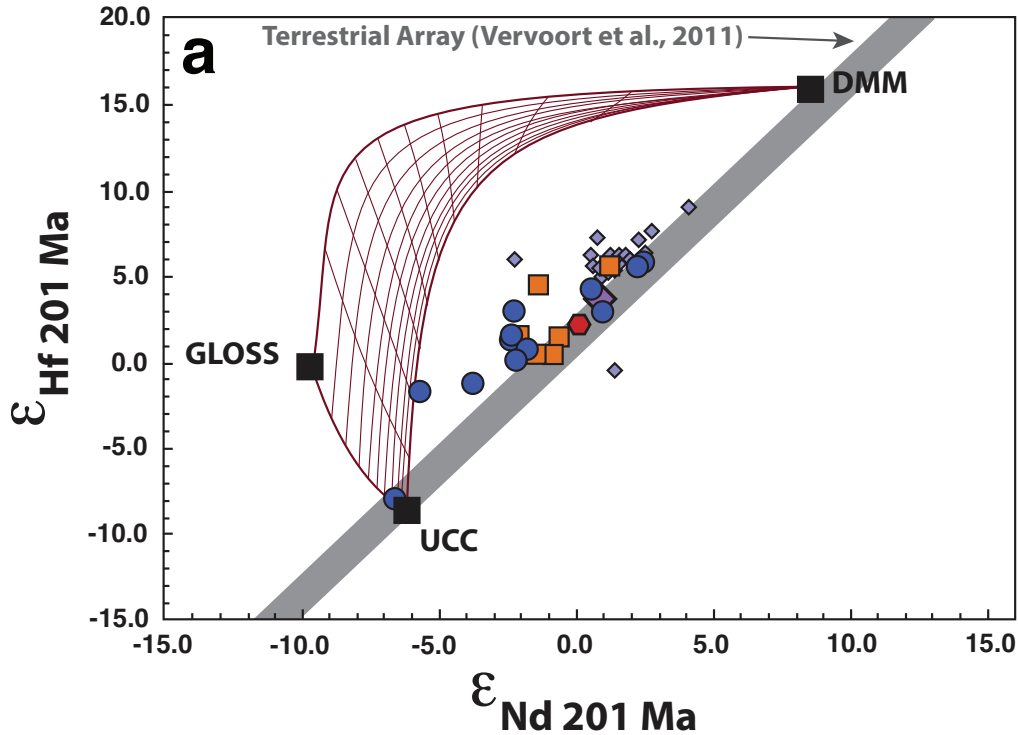


Figure 7.

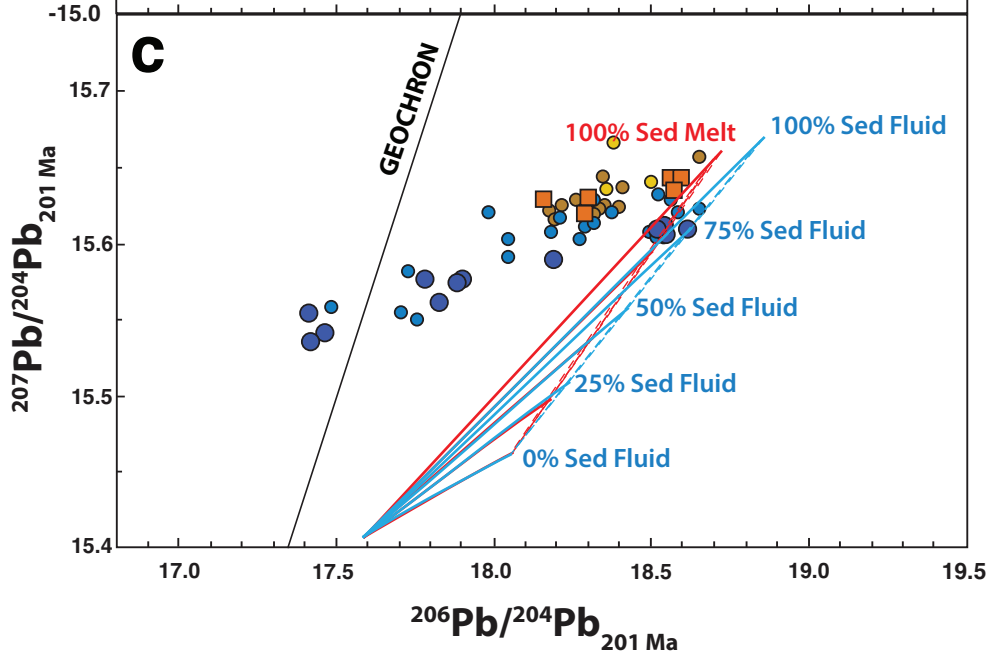
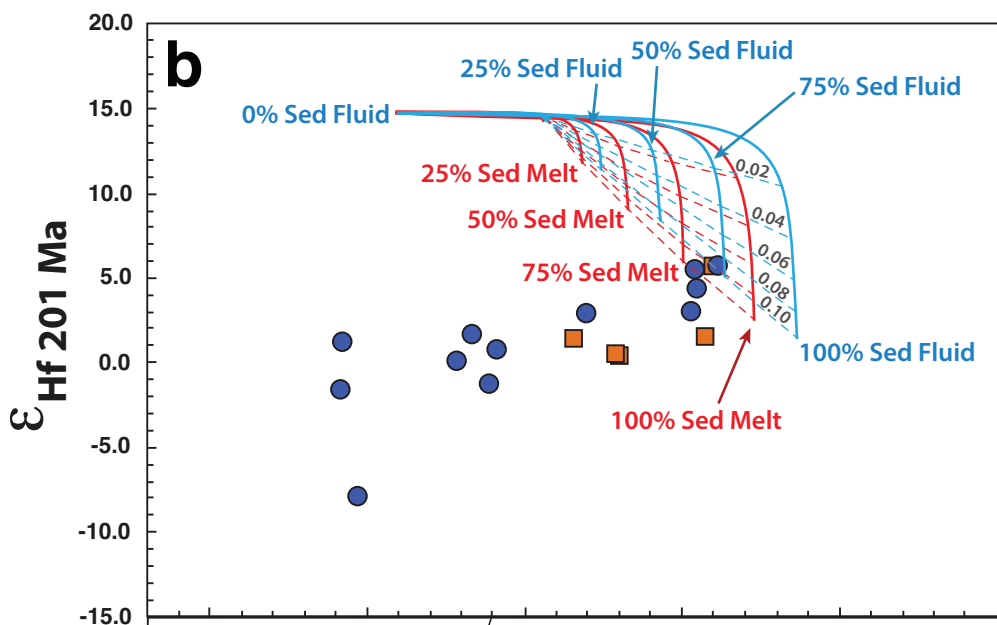
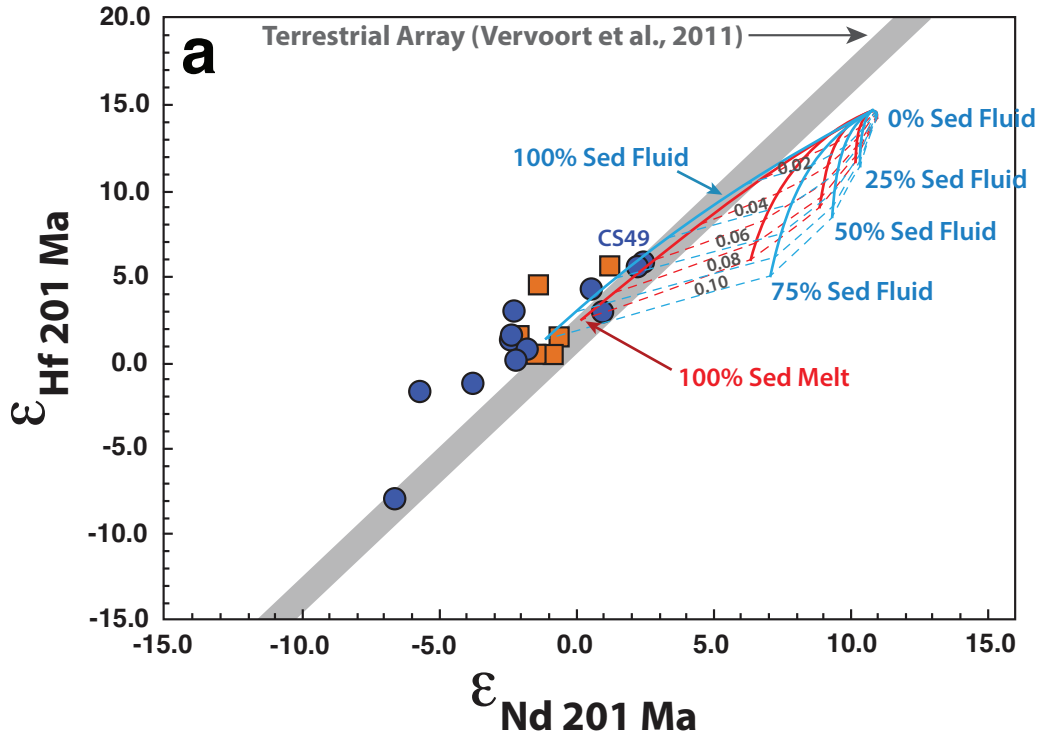


Figure 8.

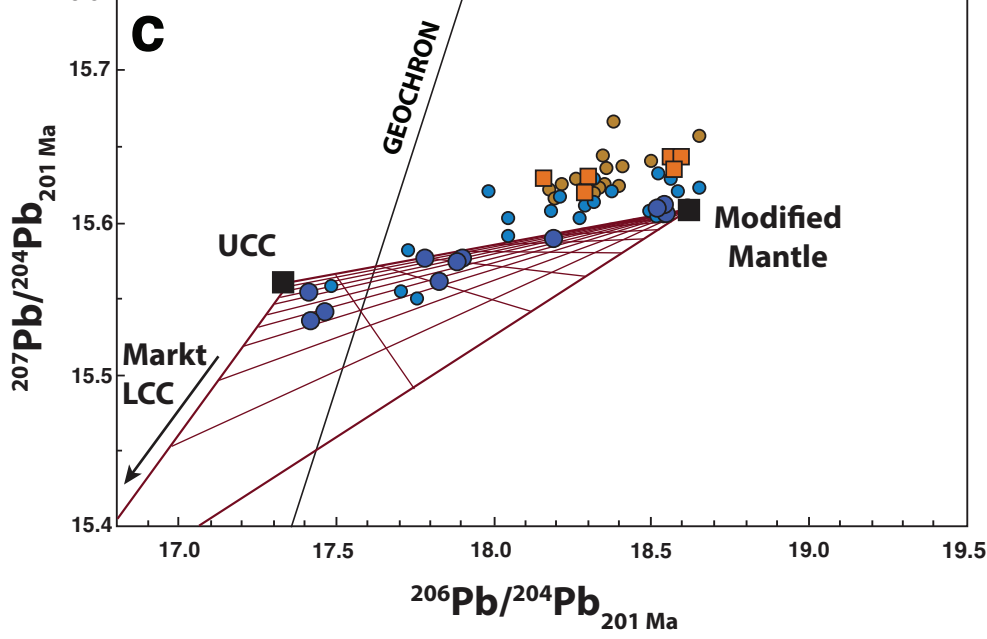
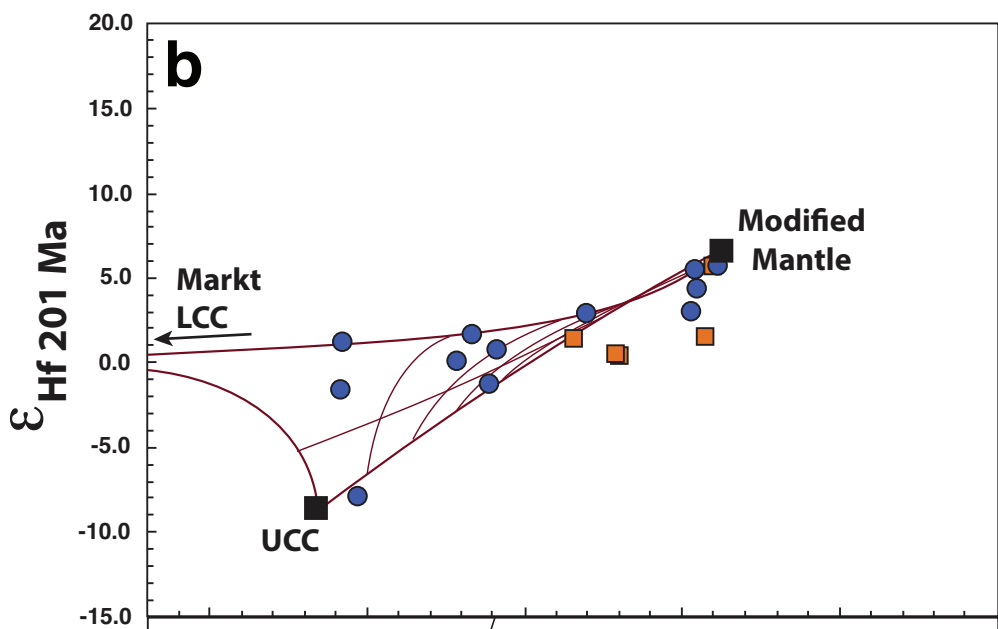
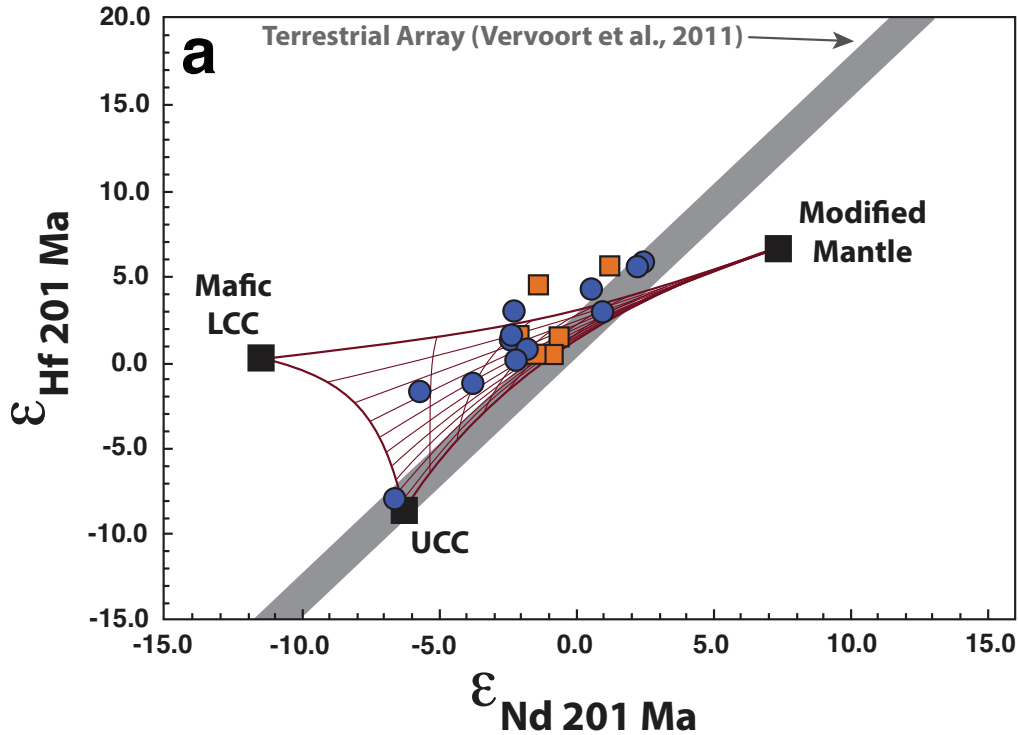


Table 1. Locations and characteristics of samples analyzed for this study, where available.

Sample name	Location description	Latitude (°N)	Longitude (°W)	Outcrop	Reference
<u>Carolinas and Southern ENA:</u>					
CS9	Georgia	34° 45' 21"	83° 29' 33"	Dike	Callegaro et al., 2013
CS26	South Carolina	34° 12' 27"	81° 03' 13"	Dike	Callegaro et al., 2013
CS23	South Carolina	34° 38' 53"	80° 31' 02"	Dike	Callegaro et al., 2013
CS28	South Carolina	34° 39' 08"	80° 31' 01"	Dike	Callegaro et al., 2013
CS14	South Carolina	34° 39' 27"	82° 01' 56"	Dike	Callegaro et al., 2013
CS41	North Carolina	34° 56' 14"	79° 49' 15"	Dike	Callegaro et al., 2013
CS48	North Carolina	35° 04' 15"	79° 50' 38"	Dike	Callegaro et al., 2013
CS46	North Carolina	35° 06' 48"	79° 48' 15"	Dike	Callegaro et al., 2013
CS55	North Carolina	35° 45' 48"	79° 02' 47"	Dike	Callegaro et al., 2013
CS57	North Carolina	35° 50' 11"	79° 00' 48"	Dike	Callegaro et al., 2013
CS49	North Carolina	36° 06' 47"	78° 46' 02"	Sill	Callegaro et al., 2013
CS73	Virginia	37° 17' 44"	78° 27' 38"	Dike	Callegaro et al., 2013
<u>Newark basin:</u>					
NEW03	Palisades Sill			Sill	Merle et al., 2014
NEW136C	Palisades Sill, olivine cumulate layer			Sill	Merle et al., 2014
NEW133	Orange Mountain flow	40° 18' 53"	75° 50' 53"	Lava Flow	Merle et al., 2014
NEW68	Preakness flow	40° 38' 50"	74° 34' 23"	Lava Flow	Merle et al., 2014
NEW52	Preakness flow	40° 40' 33"	74° 24' 32"	Lava Flow	Merle et al., 2014
NEW74	Hook Mountain flow	40° 49' 03"	74° 19' 45"	Lava Flow	Merle et al., 2014
<u>Morocco:</u>					
AN134	Tiourjidal section, basal flow	31° 07' 40"	7° 20' 46"	Lava Flow	Marzoli et al., 2004
<u>Sierra Leone:</u>					
SL45	High-TiO ₂ sample, Freetown Layered Complex, Sierra Leone				Callegaro et al., 2017

Table 2. Hafnium isotope measurements for samples analyzed in this study.

Sample name	Lu (ppm) *	Hf (ppm) *	$^{176}\text{Hf}/^{177}\text{Hf}$	2σ **	ϵ_{Hf} ^a	$^{176}\text{Hf}/^{177}\text{Hf}_{201 \text{ Ma}}$	$\epsilon_{\text{Hf}, 201 \text{ Ma}}$ ^a
<u>Carolinas and Southern ENA:</u>							
CS9	0.51	2.02	0.282879	0.000004	3.34	0.282745	3.02
CS26	0.45	1.61	0.282762	0.000004	-0.81	0.282613	-1.64
CS23	0.40	1.68	0.282908	0.000004	4.33	0.282782	4.33
CS28	0.35	1.17	0.282839	0.000003	1.93	0.282683	0.83
CS14	0.42	1.77	0.282753	0.000004	-1.14	0.282626	-1.16
CS41	0.32	0.94	0.282880	0.000004	3.35	0.282698	1.35
CS48	0.35	1.13	0.282826	0.000003	1.47	0.282664	0.17
CS46	0.43	2.54	0.282835	0.000004	1.76	0.282745	3.03
CS55	0.47	1.74	0.282960	0.000002	6.20	0.282818	5.62
CS57	0.37	1.11	0.282883	0.000004	3.46	0.282706	1.65
CS49	0.34	1.33	0.282962	0.000003	6.26	0.282825	5.86
CS73	0.38	1.54	0.282568	0.000003	-7.67	0.282437	-7.85
<u>Newark basin:</u>							
NEW03	0.29	2.95	0.282727	0.000002	-2.06	0.282674	0.53
NEW136C	0.20	1.54	0.282743	0.000004	-1.47	0.282673	0.50
NEW133	0.23	2.37	0.282754	0.000002	-1.11	0.282702	1.50
NEW68	0.25	2.22	0.282849	0.000002	2.26	0.282789	4.57
NEW52	0.35	2.07	0.282794	0.000004	0.32	0.282704	1.58
NEW74	0.62	3.00	0.282930	0.000002	5.13	0.282821	5.71
<u>Morocco:</u>							
AN134	0.31	3.66	0.282769	0.000002	-0.57	0.282724	2.27
<u>Sierra Leone:</u>							
SL45	0.05	0.16	0.282917	0.000005	4.67	0.282785	4.45

* Lutetium and Hf elemental compositions from Callegaro et al. (2013, 2017), Marzoli et al. (2004), and Merle et al. (2013).

** Uncertainties for $^{176}\text{Hf}/^{177}\text{Hf}$ measurements reported as 2σ standard errors.

^a ϵ_{Hf} values for measured results calculated using a CHUR $^{176}\text{Hf}/^{177}\text{Hf}$ ratio of 0.282785. Age-corrected ϵ_{Hf} values for 201 Ma were calculated using an adjusted CHUR $^{176}\text{Hf}/^{177}\text{Hf}$ ratio of 0.282659.